Catalytic Transfer of Magnetism using a Neutral Iridium Phenoxide Complex

Amy J. Ruddlesden,[a] Ryan E. Mewis,[a] Gary G. R. Green,[b] Adrian C. Whitwood[a] and Simon B. Duckett.*[a]

AUTHOR ADDRESS [a] Department of Chemistry, University of York, Heslington, YO10 5DD; Tel: 01904 322564; E-mail: simon.duckett@york.ac.uk, [b] York Neuroimaging Centre, The BiocentreYork, Science Park, Heslington, York, YO10 5NY.

Supplementary information

Contents

1. General experimental

Analysis. Errors were calculated using the Jackknife method, eliminating each value in turn and recalculating the activation parameters. The standard deviations were then calculated for each set of activation values and from this the standard error was calculated as described in Figure S1.[1]

Standard Deviation

$$s = \sqrt{\frac{\sum(x - \bar{x})^2}{(n-1)}}$$

where: $s =$ standard deviation

$x =$ measured values

$\bar{x} =$ sample mean

$n =$ sample size

Standard Error

$$St\ error = \frac{s(n-1)}{\sqrt{n}}$$

where: $s =$ standard deviation

$n =$ sample size

Figure S1. Calculation of standard deviation and standard error

2. Synthesis details of the synthesis of 1-(2,4,6-trimethylphenyl)-1H-imidazole, 3-(2-methylene-4-nitrophenol)-1-(2,4,6-trimethylphenyl) imidazolium bromide (L_1HBr), silver(II) 3-(2-methylene-4-nitrophenolate)-1-(2,4,6-trimethylphenyl)imidazolylidene (AgL_1) and iridium(I) (3-(2-methylene-4-nitrophenolate)-1-(2,4,6-trimethylphenyl)imidazolylidene)(cyclooctadiene) (1)

Synthesis of 1-(2,4,6-trimethylphenyl)-1H-imidazole[2]

Glacial acetic acid (10 ml), aqueous formaldehyde (3 ml, 37 wt %, 40 mmol) and aqueous glyoxal (4.6 ml, 40 wt %, 40 mmol) were added to a round bottom flask and heated at 70°C. A solution of glacial acetic acid (10 ml), ammonium acetate (3.08 g, 40 mmol, in 2 ml water) and mesitylamine (5.6 ml, 40 mmol) was added dropwise to the flask over a period of 30 min. The resulting solution was continuously stirred and heated for 18 h. The reaction mixture was cooled to room temperature and was added dropwise to a stirred solution of sodium hydrogen carbonate (29.4 g in 300 ml water). The product formed a precipitate which was filtered off and washed with water before being allowed to air dry. The brown solid was dissolved in the minimal amount of ethyl acetate and placed in a freezer o/n whereupon the required product crystallised and was isolated via filtration (4.36 g, yield 59 %); ^{1}H NMR [$CDCl_3$, 400 MHz] δ 7.44 (s, 1H, $CH_{imidazole}$), 7.24 (s, 1H, $CH_{imidazole}$), 6.98 (s, 2H, $2xCH_{mesityl}$), 6.90 (s, 1H, $CH_{imidazole}$), 2.35 (s, 3H, CH_3), 2.00 (s, 6H, $2xCH_3$); $^{13}C\{^{1}H\}$ NMR [$CDCl_3$] δ 138.8, 137.5, 135.4, 133.4, 129.5, 129.0, 120.1, 21.0 (CH_3), 17.3 ($2xCH_3$); MS [ESI] m/z 187.0 $(M+H)^+$

Synthesis of 3-(2-methylene-4-nitrophenol)-1-(2,4,6-trimethylphenyl) imidazolium bromide, L_1HBr[3]

1-(2,4,6-trimethylphenyl)-1H-imidazole (0.61 g, 3.3 mmol) and 2-hydroxy-5-nitrobenzyl bromide (0.76 g, 3.3 mmol) were dissolved in toluene (8 ml). The resulting mixture was refluxed for 18 h and then the solution was cooled to room temperature. The precipitate was collected via vacuum filtration and was washed with diethyl ether (1.25 g, yield 91 %); ^{1}H NMR [DMSO, 400 MHz] δ 11.81 (s, 1H, O*H*), 9.55 (s, 1H, $CH_{imidazole}$), 8.39 (d, 1H, ^{4}J(HH) = 2.55 Hz, $CH_{aromatic}$), 8.22 (dd, 1H, ^{4}J(HH) = 2.55 Hz, ^{3}J(HH) = 9.04 Hz, $CH_{aromatic}$), 8.05 (s, 1H, $CH_{imidazole}$), 7.94 (s, 1H, $CH_{imidazole}$), 7.15 (s, 2H, $2xCH_{mesityl}$), 7.09 (d, 1H, ^{3}J(HH) = 9.04 Hz, $CH_{aromatic}$), 5.53 (s, 2H, CH_2), 2.33 (s, 3H, CH_3), 2.01 (s, 6H, $2xCH_3$); $^{13}C\{^{1}H\}$ NMR [DMSO, 500 MHz] δ 163.3 ($C_{aromatic}$), 141.2 ($C_{aromatic}$), 140.3 ($C_{aromatic}$), 139.1 ($CH_{imidazole}$), 135.2 ($C_{aromatic}$), 132.0 ($C_{aromatic}$), 130.1 ($2xCH_{mesityl}$), 128.1 ($CH_{aromatic}$), 127.9 ($CH_{aromatic}$), 125.0 ($CH_{imidazole}$), 124.1 ($CH_{imidazole}$), 122.2 ($C_{aromatic}$), 116.7 ($CH_{aromatic}$), 49.2 (CH_2), 21.5 (CH_3), 17.7 ($2xCH_3$); MS [ESI] m/z 338.1 $(M-Br)^+$

Synthesis of silver(II) 3-(2-methylene-4-nitrophenolate)-1-(2,4,6-trimethylphenyl)imidazolylidene, AgL_1[3]

L_1 (500 mg, 1.2 mmol), silver (I) oxide (569.4 mg, 2.5 mmol) and 4Å molecular sieves (1.12 g) were added to a Schlenk flask under a nitrogen atmosphere. Dried THF (8.5 ml) and toluene (8.5 ml) were added to the flask and the reaction mixture was stirred at reflux for 3 h. Once cooled to room temperature, the mixture was diluted with dichloromethane (80 ml), filtered through a pad of celite and washed through with dichloromethane (2 x 5 ml). The solvent was removed under pressure to produce a yellow solid (0.45 g, yield 85%); ^{1}H NMR [$CDCl_3$, 400 MHz] δ 8.16 (s br, 1H, $CH_{aromatic}$), 7.78 (s br, 1H, $CH_{aromatic}$), 7.38 (s br, 1H, $CH_{aromatic}$), 7.01 (s br, 2H, $2xCH_{mesityl}$), 6.99 (s br, 1H, $CH_{aromatic}$), 5.84

(s br, 1H, $CH_{aromatic}$), 5.27 (s br, 2H, CH_2), 2.42 (s, 3H, CH_3), 1.96 (s br, 6H, 2xCH_3); $^{13}C\{^1H\}$ NMR [$CDCl_3$] δ 174.7, 139.6, 137.2, 135.2, 134.5, 129.2 (2x$CH_{mesityl}$), 127.2 ($CH_{aromatic}$), 126.8 ($CH_{aromatic}$), 124.4, 122.2, 121.9 ($CH_{aromatic}$), 121.5 ($CH_{aromatic}$), 50.3 (CH_2), 21.4 (CH_3), 17.9 (2xCH_3); MS [ESI] m/z 783 (Ag dimer, protonated phenol groups)

Synthesis of iridium(I) (3-(2-methylene-4-nitrophenolate)-1-(2,4,6-trimethylphenyl)imidazolylidene)(cyclooctadiene), 1

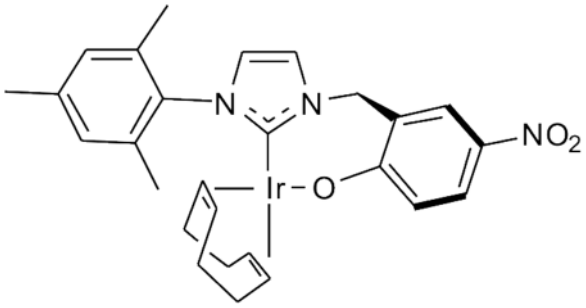

AgL_1 (170 mg, 0.38 mmol) and $[Ir(COD)Cl]_2$ (129 mg, 0.19 mmol) were added to a Schlenk flask, which was evacuated and filled with nitrogen. Dry THF (12 ml) was added to the flask and the reaction mixture was stirred overnight at room temperature. The mixture was diluted with DCM, filtered through a pad of celite then purified by column chromatography (silica, DCM:acetone 80:20). It was evaporated to dryness to produce an orange/brown powder (0.23 g, yield 96 %); ^1H NMR [CD_2Cl_2, 500 MHz, 298 K] δ 8.17 (d, 1H, ^4J(HH) = 3.05 Hz, $CH_{aromatic}$), 7.96 (dd, 1H, ^4J(HH) = 3.05 Hz, ^3J(HH) = 9.28 Hz, $CH_{aromatic}$), 7.14 (d, 1H, ^3J(HH) = 1.94 Hz, $CH_{imidazole}$), 7.03 (s, br, 2H, 2x$CH_{mesityl}$), 6.72 (d, 1H, ^3J(HH) = 1.94 Hz, $CH_{imidazole}$), 6.60 (s v. br, 1H, CH_2 linker), 6.57 (d, 1H, ^3J(HH) = 9.28 Hz, $CH_{aromatic}$), 4.79 (s v. br, 1H, CH_2 linker), 4.40 (s, v. br, 2H, 2xCH_{COD}), 3.30 (s v. br, 1H, CH_{COD}), 2.45 (s v. br, 1H, CH_{COD}), 2.39 (s, 3H, CH_3), 2.09 (s br, 4H, $CH_{2\ COD}$), 2.03 (s br, 6H, 2xCH_3), 1.58 (s br, 4H, $CH_{2\ COD}$); ^1H NMR [CD_2Cl_2, 500 MHz, 253 K] δ 8.18 (d, 1H, ^4J(HH) = 3.01 Hz, $CH_{aromatic}$), 7.96 (dd, 1H, ^4J(HH) = 3.01 Hz, ^3J(HH) = 9.24 Hz), 7.14 (d, 1H, ^3J(HH) = 1.87 Hz, $CH_{imidazole}$), 7.06 (s, 1H, $CH_{mesityl}$), 6.96 (s, 1H, $CH_{mesityl}$), 6.72 (d, 1H, ^3J(HH) = 1.87 Hz, $CH_{imidazole}$), 6.60 (d, 1H, ^2J(HH) = 14.02 Hz, CH_2 linker), 6.55 (d, 1H, ^3J(HH) = 9.24 Hz, $CH_{aromatic}$), 4.79 (d, 1H, ^2J(HH) = 14.02 Hz, CH_2 linker), 4.42 (m, 1H, CH_{COD}), 4.26 (m, 1H, CH_{COD}), 3.27 (m, 1H, CH_{COD}), 2.41 (m, 1H, CH_{COD}), 2.36 (s, 3H, CH_3), 2.20 – 2.00 (m, 4H, 2x$CH_{2\ COD}$), 2.07 (s, 3H, CH_3), 1.96 (s, 3H, CH_3), 1.68 – 1.53 (m, 4H, 2x$CH_{2\ COD}$); $^{13}C\{^1H\}$ NMR [CD_2Cl_2, 500 MHz, 253 K] δ 175.7 (C-OIr), 175.1 (C-Ir), 139.0 ($C_{aromatic}$), 136.1 ($C_{aromatic}$), 135.5 ($C_{aromatic}$), 134.4 ($C_{aromatic}$), 134.0 ($C_{aromatic}$), 129.1 ($CH_{aromatic}$), 128.4 ($CH_{aromatic}$), 127.0 ($CH_{aromatic}$), 126.3 ($CH_{aromatic}$), 123.4 ($CH_{imidazole}$), 123.2 ($C_{aromatic}$), 121.5 ($CH_{aromatic}$), 119.6 ($CH_{imidazole}$), 84.7 (CH), 84.6 (CH), 51.2 (CH_2), 49.7 (CH), 48.3 (CH), 34.5 (CH_2), 33.8 (CH_2), 28.9 (CH_2), 28.4 (CH_2), 21.0 (CH_3), 18.7 (CH_3), 17.6 (CH_3); MS [ESI] m/z 636.19. Anal. Calcd for $C_{27}H_{30}N_3O_3Ir$ (M_r = 636.77): C, 50.93; H, 4.75; N, 6.60. Found: C, 50.64; H, 4.52; N, 6.14.

3. Spectroscopic analysis of the behaviour of 1 in solution

The protons in **1** are strongly affected by temperature. At 298 K rapid motion occurs so that protons in the aliphatic range and the COD alkene protons appear very broad. Cooling to 253 K shows resolved signals in the NMR spectrum as the motion is reduced. This is shown in Figure S2.

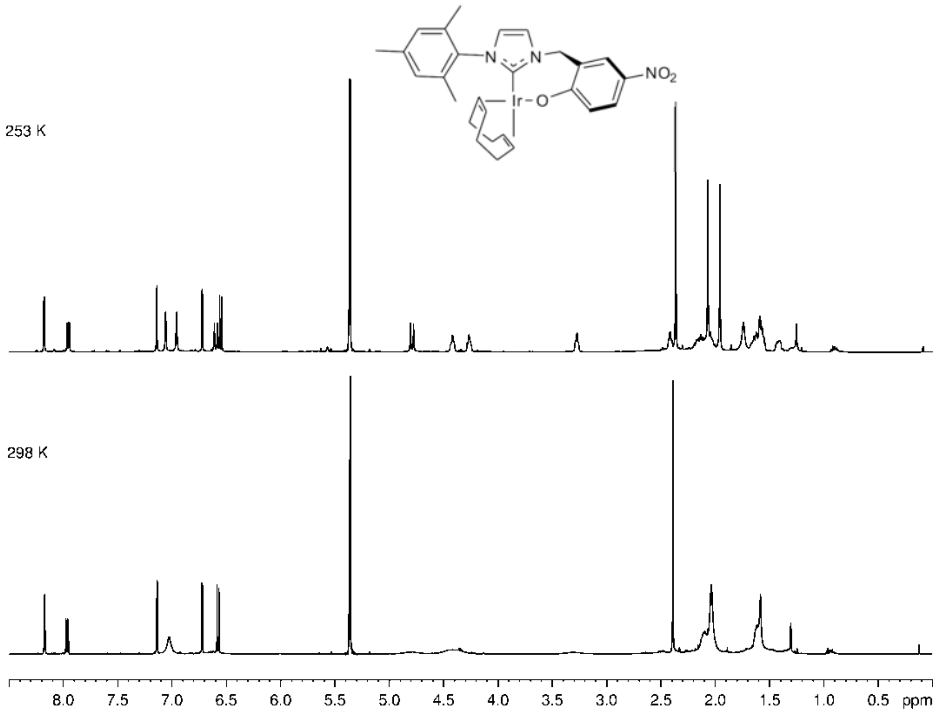

Figure S2. Comparison of ^{1}H NMR of 1 at 253 K and 298 K showing resolved peaks

Methods used in the calculation of mesityl group rates of rotation

The rapid motion causing the aromatic protons of the mesityl group to coalesce at higher temperature corresponds to rotation of this group around the single bond to the imidazole centre. This rate of rotation at different temperatures and hence calculation of the activation energy was roughly estimated by calculation from the NMR data and the linewidths of the peaks at half height as described in Figure S3. Assuming that at 248 K the exchange was very slow, then the linewidth at half the maximum peak height could be measured and the rate constants at each temperature determined.

Slow exchange $k = \pi(h_e - h_o)$

Intermediate exchange $k = \frac{\pi\sqrt{(\Delta\nu_o{}^2 - \Delta\nu_e{}^2)}}{\sqrt{2}}$

Coalescence $k = \frac{\pi\Delta\nu_o}{\sqrt{2}}$

Fast exchange $k = \frac{\pi\Delta\nu_o{}^2}{2(h_e - h_o)}$

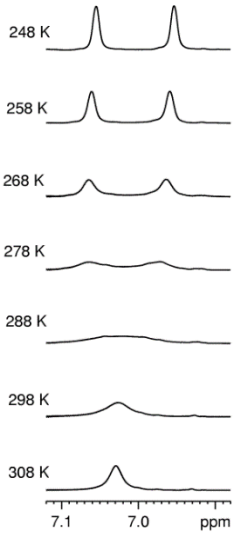

where: k = rate constant / s^{-1}

h_e = peak width at half height with exchange

h_o = peak width at half height with no exchange / 5.03 s^{-1}

$\Delta\nu_e$ = peak frequency difference with exchange

$\Delta\nu_o$ = peak frequency difference with no exchange / 50.46 s^{-1}

Figure S3. Lineshape analysis equations and corresponding ^{1}H NMR spectra for calculating rotation rates for the mestiyl group rotation

The rate constants listed in Table S1 were determined using the equations listed in Figure S3 and make the assumption that no exchange occurs at 248 K. This introduces a systematic error in the values which we estimate is no larger than 10%. Figure S4 shows the equations used to calculate the appropriate activation parameters for this rotation process and Figures S5 and S6 are the corresponding Arrhenius and Eyring-Polanyi plots.

Table S1. Experimental rate data for the mestiyl group rotation

T (K)	1/T (K^{-1})	k (s^{-1})	ln(2k / s^{-1})	ln(2k/T / s^{-1} K^{-1})
248	0.00403	0	-	-
258	0.00388	3.8	2.0	-3.5
268	0.00373	15.7	3.5	-2.1
278	0.00360	48.8	4.6	-1.2
288	0.00347	112.1	5.4	-0.3
298	0.00336	260.4	6.3	0.6
308	0.00325	766.2	7.3	1.6

Arrhenius equation:

$$k = Ae^{-E_a/RT}$$

$$\ln(k) = -\frac{E_a}{R}\left(\frac{1}{T}\right) + \ln(A)$$

where: k = rate constant / s^{-1}

E_a = Activation energy / J mol^{-1}

T = temperature / K

R = Gas constant / 8.314 J K^{-1} mol^{-1}

A = Pre-exponential factor

Eyring-Polanyi equation:

$$k = \frac{k_B T}{h} e^{-\Delta G^{\ddagger}/RT}$$

$$\ln\left(\frac{k}{T}\right) = \frac{-\Delta H^{\ddagger}}{R}\left(\frac{1}{T}\right) + \ln\left(\frac{k_B}{h}\right) + \frac{\Delta S^{\ddagger}}{R}$$

where: k = rate constant / s^{-1}

T = temperature / K

R = Gas constant / 8.314 J K^{-1} mol^{-1}

$\Delta H^{\ddagger}$ = enthalpy of activation / J mol^{-1}

$\Delta S^{\ddagger}$ = entropy of activation / J K^{-1}

h = Planck's constant /

6.626 x 10^{-34} kg m^2 s^{-1}

k_B = Boltzmann constant /

1.38 x 10^{-23} J K^{-1}

Figure S4. Arrhenius and Eyring-Polanyi equations used in this analysis

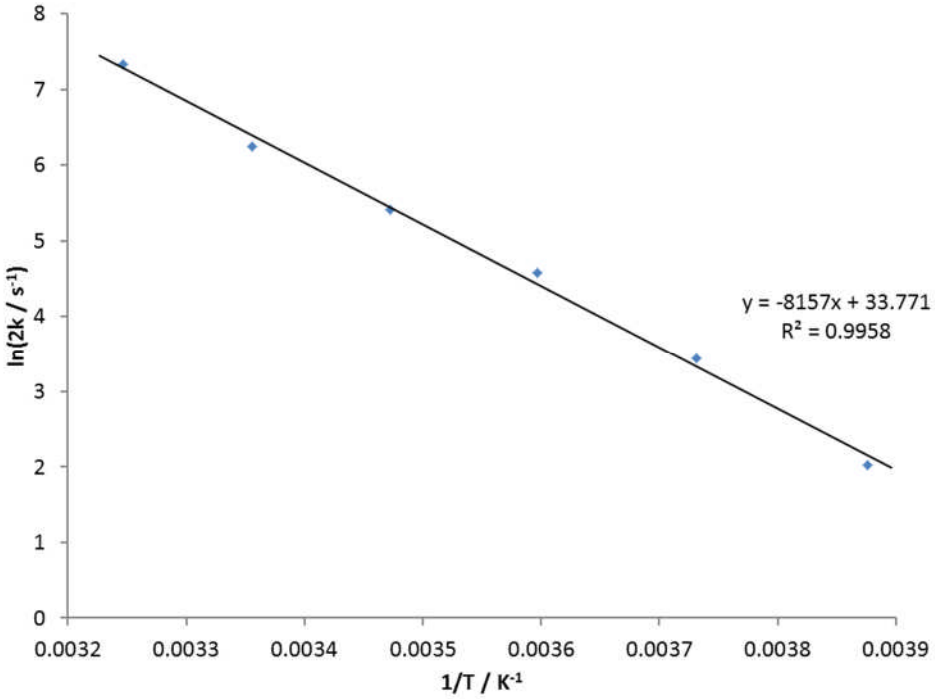

Figure S5. Arrhenius plot of experimental rate data for the mesityl rotation

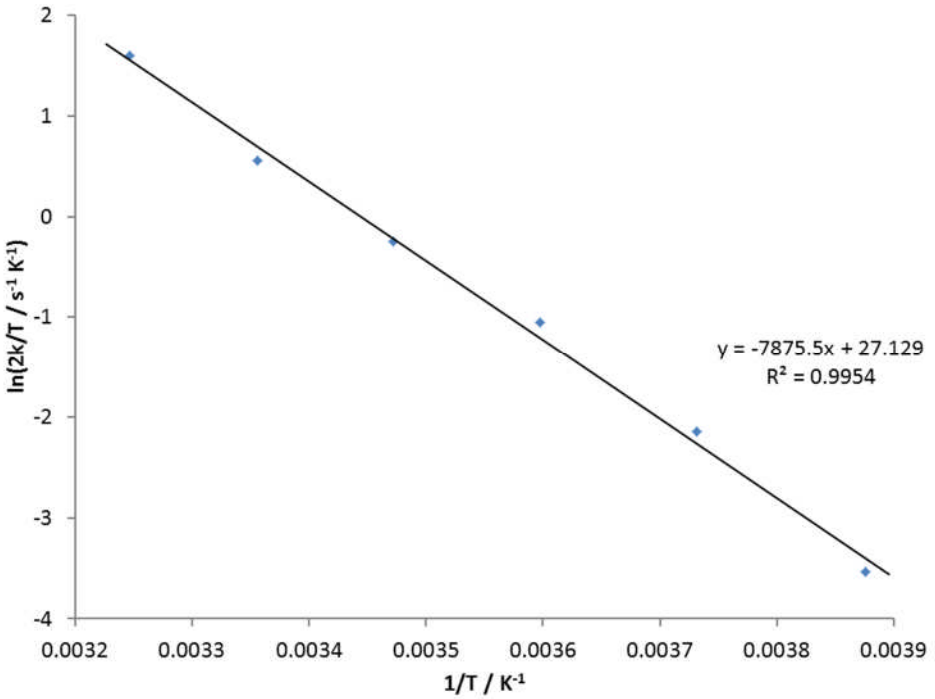

Figure S6. Eyring-Polanyi plot of experimental rate data for the mesityl rotation

Lineshape analysis of the mesityl protons using Topspin DNMR program

Lineshape analysis using the Topspin DNMR program enabled a more accurate estimate of the rate constants at differing temperatures. For the lineshape analysis, the line broadening effect was set to 3.5 Hz and the generated spectra had a 96 % agreement level with the experimental spectra. The values for the simulated exchange rates are shown in Table S2. For both the experimental data analysis and the lineshape analysis using simulated data, the two highest temperatures of 298 and 308 K were excluded from the calculations. The simulation could not be relied upon to give reliable data because the two proton peaks overlap at these higher temperatures. Therefore a value for the exchange rate could not be calculated as the simulation program only observes one peak and we note that this systematic error is not included in the error range in Figure S7. The two points were excluded from the experimental data during analysis, in order for the data sets to be comparable and include the same temperature range. The corresponding Arrhenius and Eyring-Polanyi plots are shown in Figures S7 and S8 with the determined activation parameters summarized in Table S3.

Table S2. Simulated rate data for the mestiyl group rotation

T (K)	1/T (K^{-1})	k (s^{-1})	ln(2k / s^{-1})	ln(2k/T / s^{-1} K^{-1})
248	0.00403	1.16 ± 0.05	0.84 ± 0.03	-4.67 ± 0.19
258	0.00388	5.5 ± 0.2	2.40 ± 0.10	-3.15 ± 0.13
268	0.00373	17.6 ± 0.7	3.56 ± 0.14	-2.03 ± 0.08
278	0.00360	50.3 ± 2.0	4.61 ± 0.18	-1.02 ± 0.04
288	0.00347	122.2 ± 4.9	5.50 ± 0.22	-0.16 ± 0.01
298	0.00336	2720 ± 109	8.60 ± 0.34	2.90 ± 0.12
308	0.00325	7005 ± 280	9.55 ± 0.38	3.82 ± 0.15

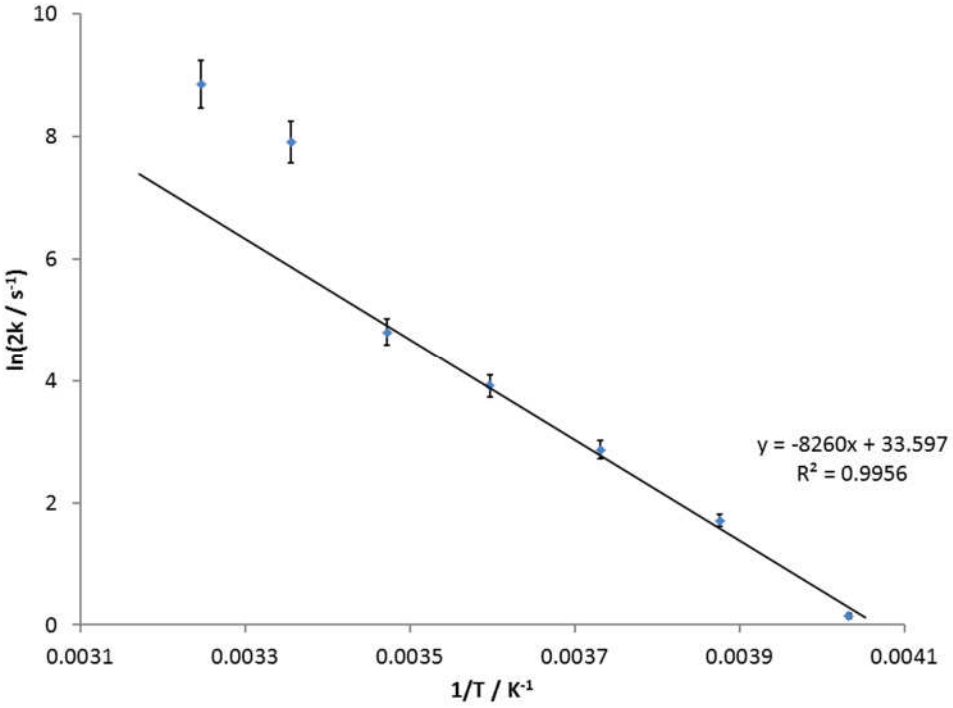

Figure S7. Arrhenius plot of simulated rate data for the mesityl rotation

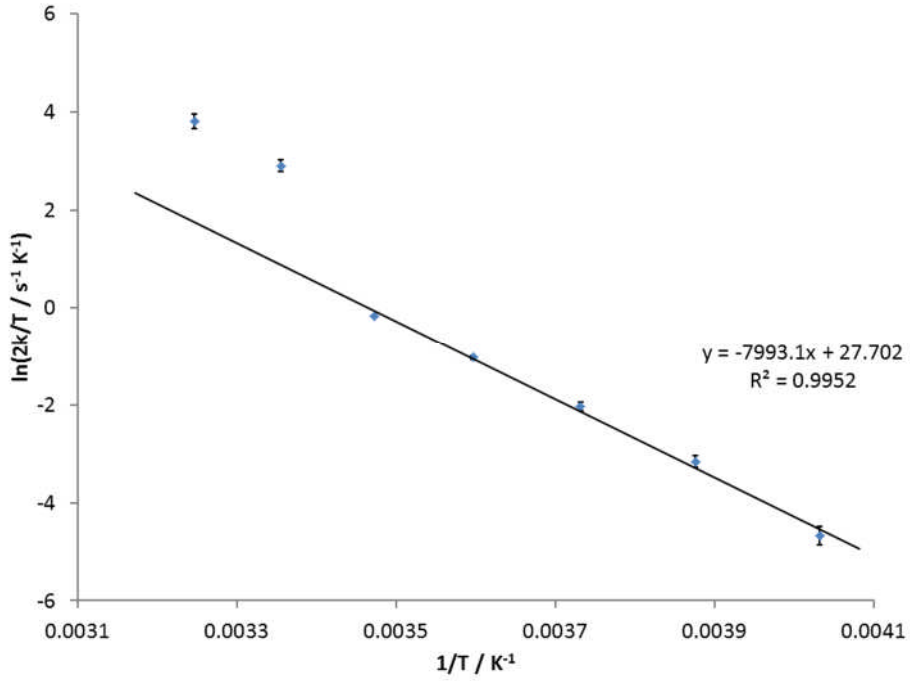

Figure S8. Eyring-Polanyi plot of simulated rate data for the mesityl rotation

Table S3. Summary of activation parameters for the experimental and simulated data for the mesityl rotation

Equation used	**Data set**	**Activation energy (E_a/$\Delta H^{\ddagger}$) / kJ mol^{-1}**	**Graph R^2 value**	**Activation entropy ($\Delta S^{\ddagger}$) / J K^{-1} mol^{-1}**	**ΔG (300 K) / kJ mol^{-1}**
Arrhenius	Experimental	67.8 ± 3.1	0.9958	-	-
	Simulated	68.7 ± 5.1	0.9956	-	-
Eyring-Polanyi	Experimental	65.5 ± 3.1	0.9954	28.0 ± 10.9	57.1 ± 1.0
	Simulated	66.5 ± 5.1	0.9952	32.8 ± 18.9	56.6 ± 1.0

Crystal structure of 1

The x-ray crystal structure of **1** is shown in Figure S9 with Tables S4 – S11 containing the corresponding structural details.

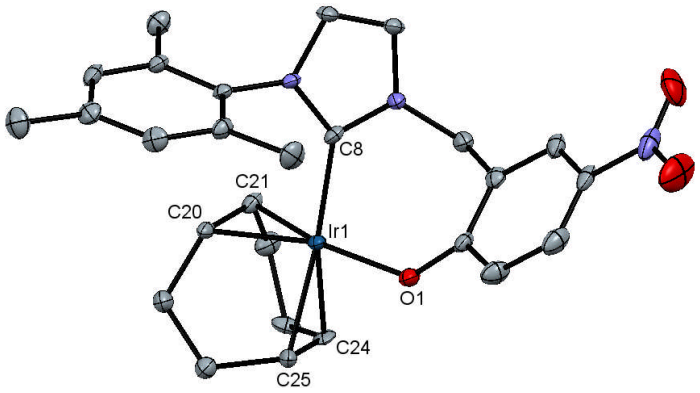

Figure S9.ORTEP plot of 1 determined at 110 K, using crystals grown by the slow diffusion of hexane into a dichloromethane solution of 1

Table S4. Crystal data and structure refinement for 1

Identification code	sbd1402
Empirical formula	$C_{27}H_{30}Ir_{1.04}N_3O_3$
Formula weight	644.77
Temperature/K	110.05(10)
Crystal system	monoclinic
Space group	$P2_1/n$
a/Å	8.7533(3)
b/Å	19.4098(11)
c/Å	13.9131(4)
α/°	90
β/°	90.472(3)
γ/°	90
Volume/Å^3	2363.77(17)
Z	4
ρ_{calc}g/cm^3	1.812

μ/mm^{-1}	5.918
F(000)	1269.0
Crystal size/mm^3	0.1894 × 0.1261 × 0.0302
Radiation	MoKα (λ = 0.71073)
2Θ range for data collection/°	5.86 to 59.996
Index ranges	-7 ≤ h ≤ 12, -23 ≤ k ≤ 27, -19 ≤ l ≤ 19
Reflections collected	12799
Independent reflections	6892 [R_{int} = 0.0326, R_{sigma} = 0.0509]
Data/restraints/parameters	6892/0/321
Goodness-of-fit on F^2	1.143
Final R indexes [I>=2σ (I)]	R_1 = 0.0345, wR_2 = 0.0675
Final R indexes [all data]	R_1 = 0.0415, wR_2 = 0.0701
Largest diff. peak/hole / e Å^{-3}	1.81/-1.39

Table S5. Fractional Atomic Coordinates (×10^4) and Equivalent Isotropic Displacement Parameters (Å^2×10^3) for sbd1402. Ueq is defined as 1/3 of of the trace of the orthogonalized UIJ tensor

Atom	x	y	z	U(eq)
Ir1	2966.0(2)	1809.2(2)	7888.6(2)	12.02(5)
O1	4920(4)	2375.2(19)	7629(2)	18.3(7)
O2	8985(5)	4766(3)	9173(3)	52.6(14)
O3	6772(5)	5187(2)	9453(3)	41.8(11)
N1	7598(5)	4727(3)	9159(3)	30.8(11)
N2	2339(4)	3011(2)	9140(2)	14.1(7)
N3	2174(4)	2128(2)	10051(2)	12.3(7)
C1	5492(5)	2926(3)	8028(3)	16.5(9)
C2	7112(5)	2979(3)	8093(3)	24.0(11)

C3	7790(6)	3566(3)	8450(3)	27.5(12)
C4	6897(6)	4106(3)	8772(3)	21.4(10)
C5	5311(6)	4070(3)	8739(3)	19.9(10)
C6	4599(5)	3487(3)	8364(3)	16.6(9)
C7	2880(5)	3447(3)	8346(3)	17.9(9)
C8	2529(4)	2324(2)	9143(3)	12.2(8)
C9	1851(5)	3252(3)	10020(3)	15.7(9)
C10	1741(5)	2697(3)	10591(3)	16.3(9)
C11	2403(5)	1450(2)	10448(3)	12.7(8)
C12	1137(5)	1059(3)	10718(3)	14.2(9)
C13	1398(5)	410(3)	11098(3)	17.7(9)
C14	2872(6)	139(3)	11216(3)	19.5(9)
C15	4097(5)	549(3)	10942(3)	20.4(10)
C16	3902(5)	1204(3)	10574(3)	16.6(9)
C17	-463(5)	1325(3)	10604(3)	21.7(10)
C18	3096(6)	-564(3)	11649(4)	26.2(11)
C19	5256(5)	1642(3)	10320(4)	25.7(11)
C20	1550(5)	955(3)	8178(3)	16.3(9)
C21	644(5)	1536(3)	7866(3)	16.5(9)
C22	-41(5)	1614(3)	6871(3)	22.5(11)
C23	1093(5)	1438(3)	6069(3)	20.3(10)
C24	2715(6)	1611(3)	6349(3)	21.8(10)
C25	3732(5)	1132(2)	6736(3)	16.0(9)
C26	3280(5)	393(3)	6938(3)	18.9(9)
C27	1830(6)	332(3)	7546(3)	20.6(10)

Ir1A	1603(8)	1783(3)	7966(4)	37(2)

Table S6. Anisotropic Displacement Parameters ($Å^2×10^3$) for sbd1402. The Anisotropic displacement factor exponent takes the form: $-2\pi^2[h^2a^{*2}U_{11}+2hka^*b^*U_{12}+\ldots]$

Atom	U_{11}	U_{22}	U_{33}	U_{23}	U_{13}	U_{12}
Ir1	14.66(8)	12.75(8)	8.69(6)	-1.43(7)	2.72(5)	-2.05(7)
O1	20.1(16)	20.0(19)	14.9(14)	-4.5(14)	5.5(12)	-5.6(13)
O2	43(3)	70(4)	44(3)	-14(3)	4(2)	-39(3)
O3	56(3)	24(2)	45(2)	-7(2)	-10(2)	-14(2)
N1	39(3)	36(3)	17.4(19)	4(2)	-1.7(17)	-23(2)
N2	19.1(18)	12.6(19)	10.7(15)	-0.5(14)	1.9(13)	-2.3(14)
N3	11.7(16)	15.6(19)	9.6(15)	-2.4(14)	3.1(12)	-1.4(15)
C1	19(2)	18(2)	12.3(19)	0.3(18)	3.6(16)	-7.7(18)
C2	18(2)	33(3)	21(2)	-3(2)	3.6(17)	-6(2)
C3	22(2)	41(4)	20(2)	0(2)	1.3(18)	-14(2)
C4	27(2)	26(3)	11.0(18)	4.2(19)	0.0(17)	-15(2)
C5	28(2)	19(3)	12.7(19)	3.6(19)	0.4(17)	-8(2)
C6	21(2)	19(2)	10.1(18)	1.9(18)	0.1(16)	-3.6(18)
C7	23(2)	14(2)	17(2)	0.2(18)	2.9(17)	0.0(19)
C8	12.8(19)	15(2)	8.9(17)	1.9(17)	1.5(14)	-1.9(16)
C9	17(2)	16(2)	14.8(18)	-5.4(18)	4.6(15)	-0.7(18)
C10	20(2)	17(2)	12.5(18)	-5.8(18)	4.9(15)	-0.5(18)
C11	16(2)	15(2)	7.6(16)	-0.7(16)	2.1(14)	-1.0(16)
C12	15(2)	17(2)	10.5(17)	-0.6(17)	2.9(15)	-2.0(17)
C13	20(2)	21(3)	12.4(19)	1.7(19)	2.4(15)	-9.1(19)
C14	25(2)	21(3)	12.3(18)	2.7(18)	0.2(17)	1(2)

C15	19(2)	25(3)	17(2)	3(2)	-3.0(17)	6(2)
C16	14(2)	22(3)	14.0(19)	-3.2(19)	1.2(15)	-5.2(18)
C17	18(2)	27(3)	20(2)	1(2)	0.5(17)	-3(2)
C18	29(3)	21(3)	29(2)	4(2)	-6(2)	1(2)
C19	15(2)	30(3)	33(3)	-1(2)	3.7(18)	-6(2)
C20	21(2)	15(2)	13.2(18)	-4.3(18)	6.9(15)	-7.4(18)
C21	13(2)	23(3)	13.5(19)	-0.8(19)	0.1(16)	-9.8(19)
C22	18(2)	31(3)	19(2)	-2(2)	0.1(17)	-2(2)
C23	25(2)	22(3)	13.7(19)	-9.7(19)	-2.2(17)	2(2)
C24	38(3)	19(3)	8.3(18)	-0.3(18)	8.7(18)	-2(2)
C25	22(2)	12(2)	13.9(19)	-2.5(17)	7.3(16)	-4.1(18)
C26	22(2)	17(2)	18(2)	-0.5(19)	3.1(16)	-3.0(19)
C27	27(2)	14(2)	21(2)	-2.4(19)	6.5(18)	-3.7(19)
Ir1A	64(5)	17(3)	31(3)	-14(2)	3(2)	2(3)

Table S7. Bond lengths for 1

Atom	Atom	Length/Å		Atom	Atom	Length/Å
Ir1	O1	2.067(3)		C5	C6	1.390(7)
Ir1	C8	2.049(4)		C6	C7	1.506(7)
Ir1	C20	2.111(5)		C9	C10	1.342(7)
Ir1	C21	2.101(5)		C11	C12	1.398(6)
Ir1	C24	2.185(4)		C11	C16	1.406(6)
Ir1	C25	2.183(4)		C12	C13	1.383(7)
O1	C1	1.303(6)		C12	C17	1.500(6)
O2	N1	1.216(6)		C13	C14	1.402(7)
O3	N1	1.222(7)		C14	C15	1.391(7)

N1	C4	1.453(7)		C14	C18	1.503(7)
N2	C7	1.474(6)		C15	C16	1.379(7)
N2	C8	1.344(6)		C16	C19	1.504(6)
N2	C9	1.382(5)		C20	C21	1.444(7)
N3	C8	1.358(5)		C20	C27	1.517(6)
N3	C10	1.391(6)		C21	C22	1.511(6)
N3	C11	1.439(6)		C22	C23	1.538(6)
C1	C2	1.424(6)		C23	C24	1.508(7)
C1	C6	1.423(7)		C24	C25	1.393(7)
C2	C3	1.375(7)		C25	C26	1.514(7)
C3	C4	1.384(8)		C26	C27	1.535(6)
C4	C5	1.391(7)				

Table S8. Bond Angles for 1

Atom	**Atom**	**Atom**	**Angle/°**		**Atom**	**Atom**	**Atom**	**Angle/°**
O1	Ir1	C20	159.87(16)		N2	C7	C6	110.1(4)
O1	Ir1	C21	158.95(17)		N2	C8	Ir1	120.3(3)
O1	Ir1	C24	89.92(16)		N2	C8	N3	104.6(4)
O1	Ir1	C25	86.12(15)		N3	C8	Ir1	134.5(4)
C8	Ir1	O1	92.88(14)		C10	C9	N2	106.0(4)
C8	Ir1	C20	96.10(17)		C9	C10	N3	107.3(4)
C8	Ir1	C21	87.03(17)		C12	C11	N3	119.4(4)
C8	Ir1	C24	154.46(18)		C12	C11	C16	121.5(4)
C8	Ir1	C25	168.35(17)		C16	C11	N3	119.1(4)
C20	Ir1	C24	89.69(18)		C11	C12	C17	121.7(4)
C20	Ir1	C25	81.46(17)		C13	C12	C11	117.9(4)

C21	Ir1	C20	40.10(19)	C13	C12	C17	120.4(4)
C21	Ir1	C24	81.48(18)	C12	C13	C14	122.4(4)
C21	Ir1	C25	98.06(18)	C13	C14	C18	120.3(4)
C25	Ir1	C24	37.19(18)	C15	C14	C13	117.6(4)
C1	O1	Ir1	132.6(3)	C15	C14	C18	122.1(4)
O2	N1	O3	122.8(5)	C16	C15	C14	122.4(4)
O2	N1	C4	118.5(6)	C11	C16	C19	121.0(5)
O3	N1	C4	118.7(5)	C15	C16	C11	118.2(4)
C8	N2	C7	122.1(4)	C15	C16	C19	120.8(4)
C8	N2	C9	111.9(4)	C21	C20	Ir1	69.6(3)
C9	N2	C7	125.0(4)	C21	C20	C27	122.7(4)
C8	N3	C10	110.2(4)	C27	C20	Ir1	114.7(3)
C8	N3	C11	125.5(4)	C20	C21	Ir1	70.3(2)
C10	N3	C11	123.8(3)	C20	C21	C22	124.5(4)
O1	C1	C2	117.8(5)	C22	C21	Ir1	111.4(3)
O1	C1	C6	123.9(4)	C21	C22	C23	112.9(4)
C6	C1	C2	118.2(5)	C24	C23	C22	112.0(4)
C3	C2	C1	120.7(5)	C23	C24	Ir1	112.3(3)
C2	C3	C4	120.0(5)	C25	C24	Ir1	71.3(3)
C3	C4	N1	120.7(5)	C25	C24	C23	123.2(5)
C3	C4	C5	121.2(5)	C24	C25	Ir1	71.5(3)
C5	C4	N1	118.2(5)	C24	C25	C26	122.5(4)
C6	C5	C4	119.8(5)	C26	C25	Ir1	110.6(3)
C1	C6	C7	120.4(4)	C25	C26	C27	113.2(4)
C5	C6	C1	120.0(4)	C20	C27	C26	113.4(4)

C5	C6	C7	119.6(5)					

Table S9. Torsion Angles for 1

A	B	C	D	Angle/°		A	B	C	D	Angle/°
Ir1	O1	C1	C2	145.6(4)		C8	N3	C10	C9	-1.0(5)
Ir1	O1	C1	C6	-37.3(7)		C8	N3	C11	C12	-115.5(5)
Ir1	C20	C21	C22	103.0(4)		C8	N3	C11	C16	65.7(5)
Ir1	C20	C27	C26	10.3(5)		C9	N2	C7	C6	96.3(5)
Ir1	C21	C22	C23	34.7(6)		C9	N2	C8	Ir1	171.8(3)
Ir1	C24	C25	C26	103.1(4)		C9	N2	C8	N3	-0.8(5)
Ir1	C25	C26	C27	28.4(5)		C10	N3	C8	Ir1	-169.9(3)
O1	C1	C2	C3	175.7(4)		C10	N3	C8	N2	1.1(5)
O1	C1	C6	C5	-176.8(4)		C10	N3	C11	C12	73.4(5)
O1	C1	C6	C7	5.1(7)		C10	N3	C11	C16	-105.3(5)
O2	N1	C4	C3	1.5(7)		C11	N3	C8	Ir1	18.0(6)
O2	N1	C4	C5	-178.7(5)		C11	N3	C8	N2	-171.0(4)
O3	N1	C4	C3	-178.6(5)		C11	N3	C10	C9	171.2(4)
O3	N1	C4	C5	1.2(7)		C11	C12	C13	C14	-0.1(7)
N1	C4	C5	C6	179.3(4)		C12	C11	C16	C15	2.3(6)
N2	C9	C10	N3	0.4(5)		C12	C11	C16	C19	-177.4(4)
N3	C11	C12	C13	-180.0(4)		C12	C13	C14	C15	0.4(7)
N3	C11	C12	C17	0.1(6)		C12	C13	C14	C18	178.9(4)
N3	C11	C16	C15	-179.0(4)		C13	C14	C15	C16	0.7(7)
N3	C11	C16	C19	1.3(6)		C14	C15	C16	C11	-2.0(7)
C1	C2	C3	C4	1.6(7)		C14	C15	C16	C19	177.7(4)
C1	C6	C7	N2	76.7(5)		C16	C11	C12	C13	-1.3(6)

C2	C1	C6	C5	0.3(6)	C16	C11	C12	C17	178.8(4)
C2	C1	C6	C7	-177.8(4)	C17	C12	C13	C14	179.8(4)
C2	C3	C4	N1	179.4(4)	C18	C14	C15	C16	-177.8(4)
C2	C3	C4	C5	-0.3(7)	C20	C21	C22	C23	-45.5(7)
C3	C4	C5	C6	-1.0(7)	C21	C20	C27	C26	91.0(5)
C4	C5	C6	C1	0.9(7)	C21	C22	C23	C24	-31.8(6)
C4	C5	C6	C7	179.0(4)	C22	C23	C24	Ir1	14.0(6)
C5	C6	C7	N2	-101.4(5)	C22	C23	C24	C25	95.7(5)
C6	C1	C2	C3	-1.6(7)	C23	C24	C25	Ir1	-104.9(4)
C7	N2	C8	Ir1	-19.2(5)	C23	C24	C25	C26	-1.8(6)
C7	N2	C8	N3	168.3(4)	C24	C25	C26	C27	-52.2(6)
C7	N2	C9	C10	-168.5(4)	C25	C26	C27	C20	-25.8(6)
C8	N2	C7	C6	-71.3(5)	C27	C20	C21	Ir1	-106.9(4)
C8	N2	C9	C10	0.2(5)	C27	C20	C21	C22	-3.9(7)

Table S10. Hydrogen Atom Coordinates (Å×10^4) and Isotropic Displacement Parameters (Å^2×10^3) for 1

Atom	x	y	z	U(eq)
H2	7731	2606	7889	29
H3	8872	3601	8474	33
H5	4715	4442	8973	24
H7A	2445	3915	8407	22
H7B	2532	3251	7724	22
H9	1638	3717	10188	19
H10	1425	2694	11243	20
H13	548	139	11285	21
H15	5104	372	11010	24

H17A	-1181	938	10605	33
H17B	-555	1575	9994	33
H17C	-697	1637	11137	33
H18A	4107	-740	11476	39
H18B	2307	-877	11402	39
H18C	3021	-533	12350	39
H19A	6200	1393	10477	39
H19B	5223	2073	10686	39
H19C	5229	1745	9630	39
H20	1452	845	8877	20
H21	28	1754	8387	20
H22A	-395	2095	6785	27
H22B	-943	1309	6813	27
H23A	1022	940	5921	24
H23B	810	1696	5481	24
H24	3204	1966	5930	26
H25	4820	1196	6544	19
H26A	4133	160	7278	23
H26B	3111	152	6319	23
H27A	940	267	7113	25
H27B	1915	-82	7958	25

Table S11. Atomic Occupancy for 1

Atom	Occupancy
Ir1A	0.0418(12)

4. Reactivity of 1 towards hydrogen and pyridine

Activation of 1 with hydrogen to form 2

Reaction of **1** with H_2 proceeds according to Figure S10 to form **2**. Figure S11 portrays a series of ^1H NMR spectra showing how the activation step can be controlled by temperature and confirms that **2** is highly fluxional.

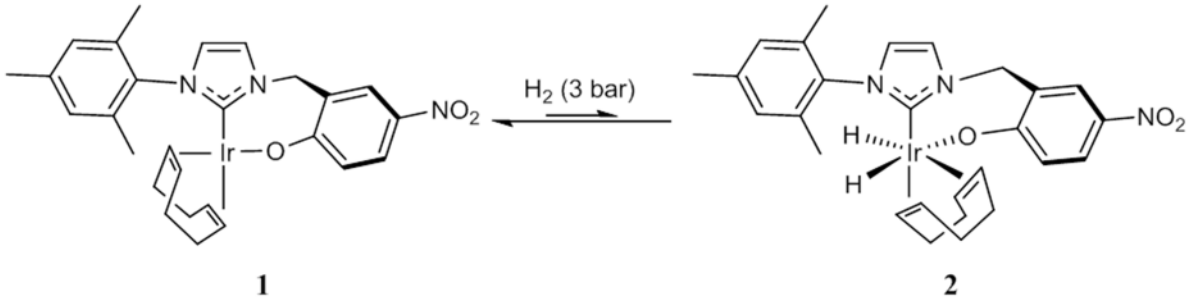

Figure S10. Structure of 2 (overall 5% yield) which demonstrates reversible hydrogen addition and results from the oxidative addition of H_2 to 1 in CD_2Cl_2 at 253 K

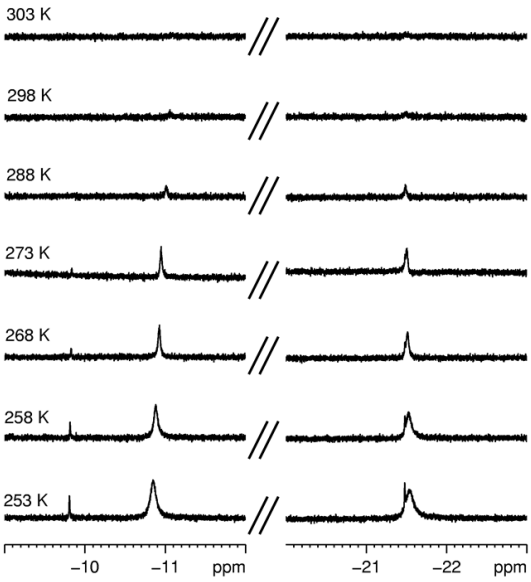

Figure S11. Hydride region of 1 in the presence of hydrogen

Addition of pyridine and hydrogen and analysis of the active complex, 3

When **1** reacts with pyridine and H_2, a new product, **3** is formed. Figure S12 shows how this reaction results in the loss of signals for **1** and the growth of **3** over a time course of 17 days as detailed in Table S12. Figure S13 shows the structure of **3** and Table S13 details the characterization data with Figure S14 showing how NOESY NMR spectroscopy was used to aid these assignments.

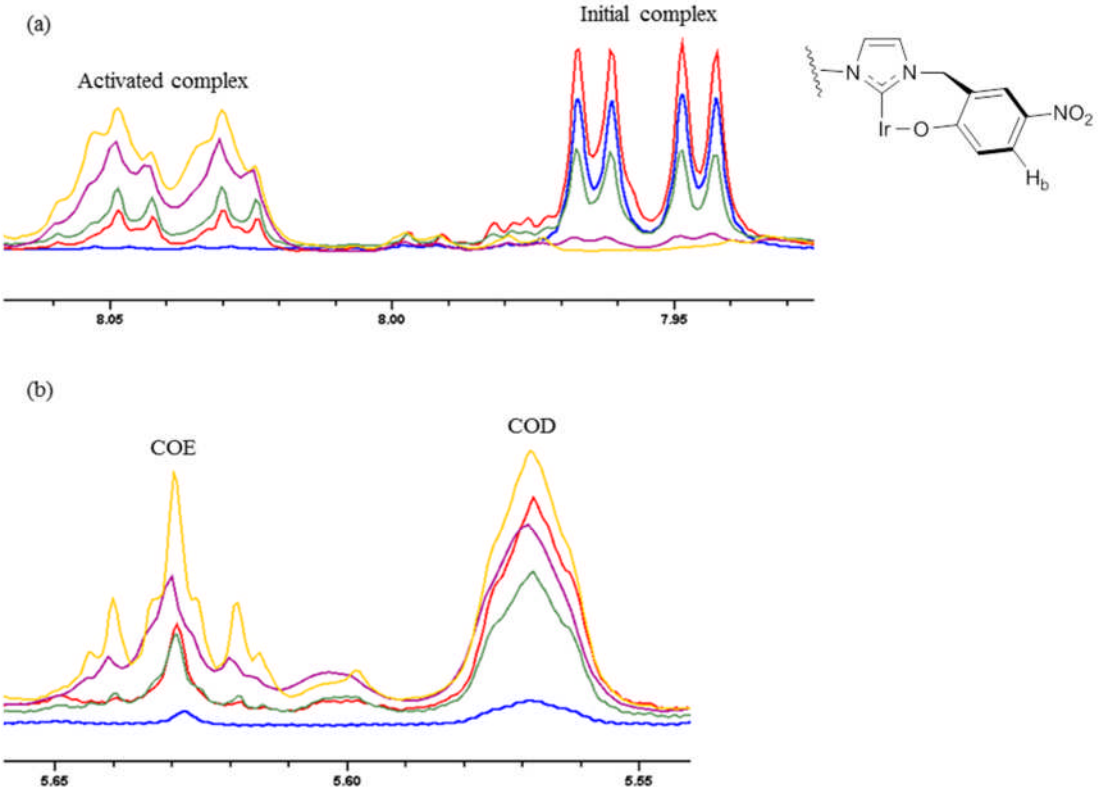

Figure S12. Evolution of spectra as 1 undergoes slow activation to 3 and releases COD into solution, showing (a) carbene H_b signal and (b) COD and COE

Table S12. Ratios showing how the concentrations of cyclooctadiene, cyclooctene, initial carbene and activated carbene vary over time

	Integrals during activation		Complex percentages (%)	
	Free COD (δ 5.57)	**Cyclooctene (δ 5.63)**	**Initial complex H_b dd (δ 7.95)**	**Activated complex H_b dd (δ 8.04)**
Initial complex	0.168	0.064	100	0
6 hours	0.817	0.278	78	22
24 hours	1.307	0.630	60	40

6 days	1.581	1.128	25	75
17 days	2.012	1.517	0	100

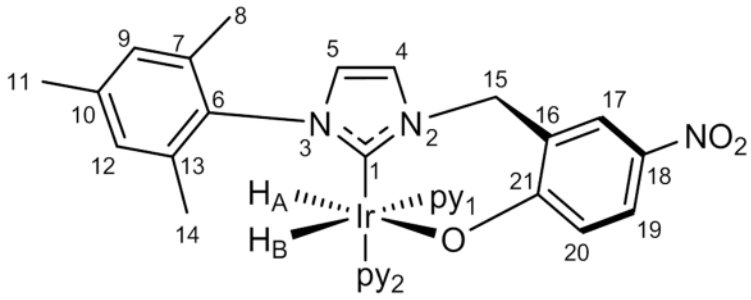

Figure S13. Active complex, 3_A, with assignments

Table S13. Characterisation data for 3_A with pyridine and hydrogen in CD_2Cl_2 at 233 K (NMR, 500 MHz)

Position	^{1}H δ / ppm	^{13}C{^{1}H} δ / ppm	^{15}N δ / ppm
1		175.5	
2			190.9
3			192.5
4	7.19, d, ^{3}J(HH) = 1.48 Hz	120.0	
5	6.61, d, ^{3}J(HH) = 1.48 Hz	120.5	
6		137.9	
7		137.0	
8	2.31, s	21.0	
9	6.46, s	128.1	
10		136.0	
11	0.93, s	16.6	
12	7.01, s	128.7	
13		136.5	
14	2.16, s	25.3	

15	4.46, 6.48, both d, ^{2}J(HH) = 13.55 Hz	51.7	
16		124.8	
17	8.17, d, ^{4}J(HH) = 2.82 Hz	127.2	
18		132.3	
19	8.04, dd, ^{4}J(HH) = 2.82 Hz, ^{3}J(HH) = 9.04 Hz	126.9	
20	6.69, d, ^{3}J(HH) = 9.04 Hz	122.2	
21		177.7	
H_A	-21.4, d, ^{2}J(HH) = 8.90 Hz		
H_B	-28.9, d, ^{2}J(HH) = 8.90 Hz		
py_{eq} *o, m, p*	8.13, 6.92, 7.60, all m	152.8, 124.5, 135.5	258.4
py_{ax} *o, m, p*	8.92, 7.11, 7.66, all m	154.6, 124.7, 135.8	240.7

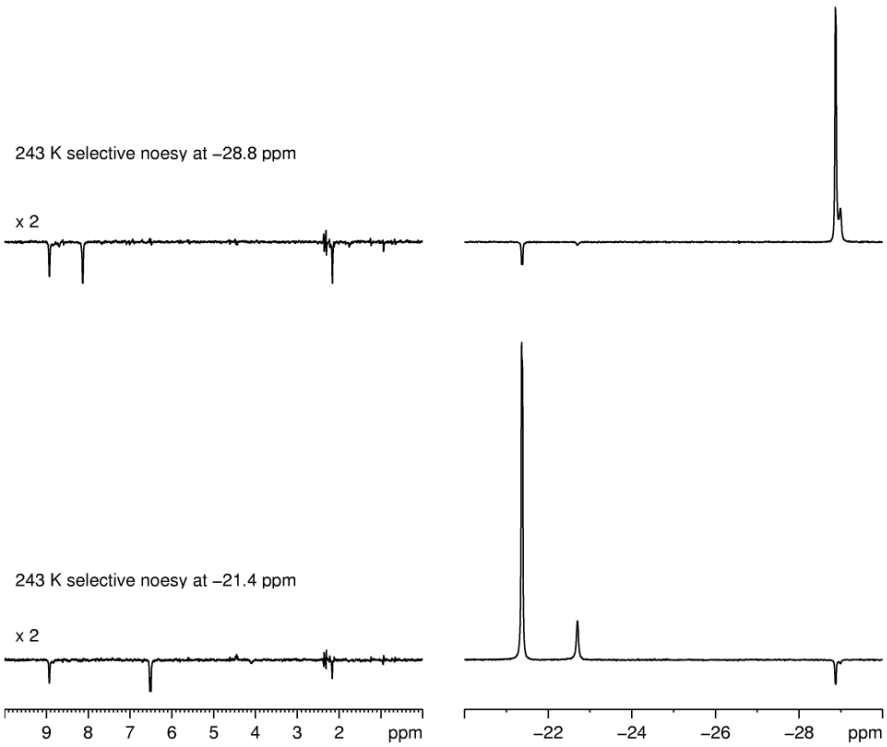

Figure S14. EXSY spectra at 243 K showing coupling between the hydrides and bound pyridine. H_A shows an NOE interaction with the py_{ax} ortho ^1H signal and H_B shows an NOE interaction with the py_{ax} ortho ^1H signal as well as the py_{eq} ortho ^1H signal. No exchange is observed at 243 K between the hydrides and free hydrogen

UV-Vis analysis

1 has a strong yellow/orange colour when in solution which is retained upon activation with pyridine and H_2. UV-vis analysis of **1** in DCM gives a strong absorption band at 405.5 nm. From this, the molar absorption coefficient, ε, can be calculated using the absorbance of a solution of known concentration.

$$A = \varepsilon c l$$

where: A = absorbance

ε = molar absorption coefficient / $dm^3\ mol^{-1}\ cm^{-1}$

l = cell path length / 1 cm

For a DCM solution of **1** the value of ε was calculated to be 21060 $dm^3\ mol^{-1}\ cm^{-1}$.

$$\varepsilon = \frac{0.4965}{2.36 \times 10^{-5}\ mol\ dm^{-3} \times 1\ cm} = 21060\ dm^3\ mol^{-1}\ cm^{-1}$$

Analysis of the activated complex, **3**, gives a strong absorption band at 398.6 nm with ε = 10975 $dm^3\ mol^{-1}\ cm^{-1}$.

$$\varepsilon = \frac{0.5180}{4.72 \times 10^{-5}\ mol\ dm^{-3} \times 1\ cm} = 10975\ dm^3\ mol^{-1}\ cm^{-1}$$

These values are consistent with the intense colour being caused by a charge transfer band. Figure S15 shows the UV-vis spectra and demonstrates that pyridine does not absorb in the region between 350 and 450 nm and therefore the absorption band in **3** is due to the complex itself and not excess pyridine in solution.

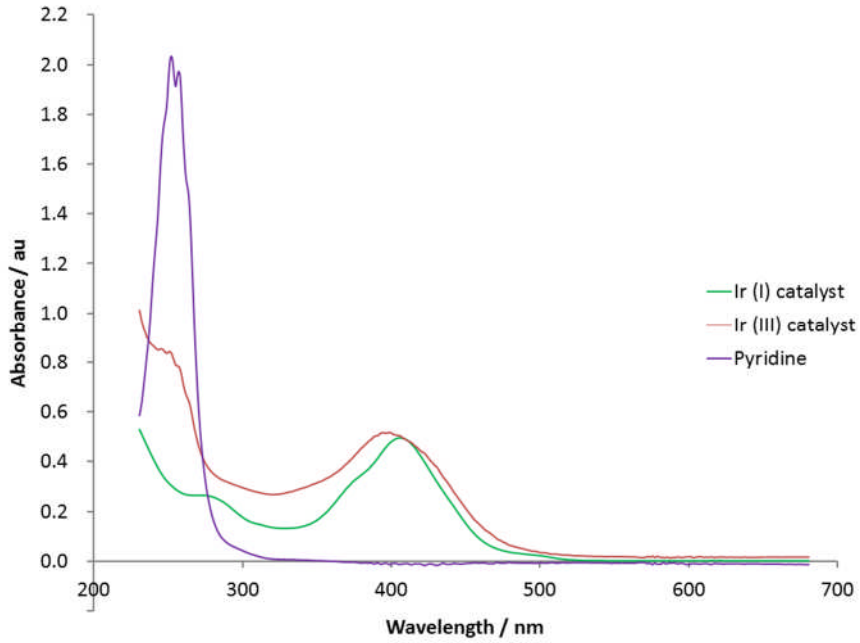

Figure S15. UV-vis spectra of 1, 3 and pyridine in DCM

The UV-vis spectra of **1** and **3** can be compared to that of **4** which is yellow when dissolved in methanol, with an absorption band at 427.0 nm and an absorption of 0.1419 for a solution of concentration equal to 6.87 x 10^{-5} mol dm^{-3}.

$$\varepsilon = \frac{0.1419}{6.87 \times 10^{-5}\, mol\, dm^{-3} \times 1\, cm} = 2065\, dm^3\, mol^{-1}\, cm^{-1}$$

Upon activation of **4** to $[Ir(IMes)(H)_2(py)_3]Cl$ in methanol, the bright yellow colour disappears and instead the solution appears to have only a very faint yellow tinge. Analysis of the activated complex, $[Ir(IMes)(H)_2(py)_3]Cl$, at 427.0 nm gives an absorption of 0.0144 with an absorption coefficient of 230 dm^3 mol^{-1} cm^{-1}. This much lower absorption coefficient is expected because the solution no longer absorbs in the visible region so no longer appears colored.

$$\varepsilon = \frac{0.0144}{6.25 \times 10^{-5}\, mol\, dm^{-3} \times 1\, cm} = 230\, dm^3\, mol^{-1}\, cm^{-1}$$

Now, the maximum absorption is shifted into the UV region of the spectrum as shown in Figure S16 and a very broad signal appears at approximately 341.0 nm with an absorbance of 0.2133 and a ε of 3413 dm^3 mol^{-1} cm^{-1} which is much larger than at 427.0 nm.

$$\varepsilon = \frac{0.2133}{6.25 \times 10^{-5}\, mol\, dm^{-3} \times 1\, cm} = 3413\, dm^3\, mol^{-1}\, cm^{-1}$$

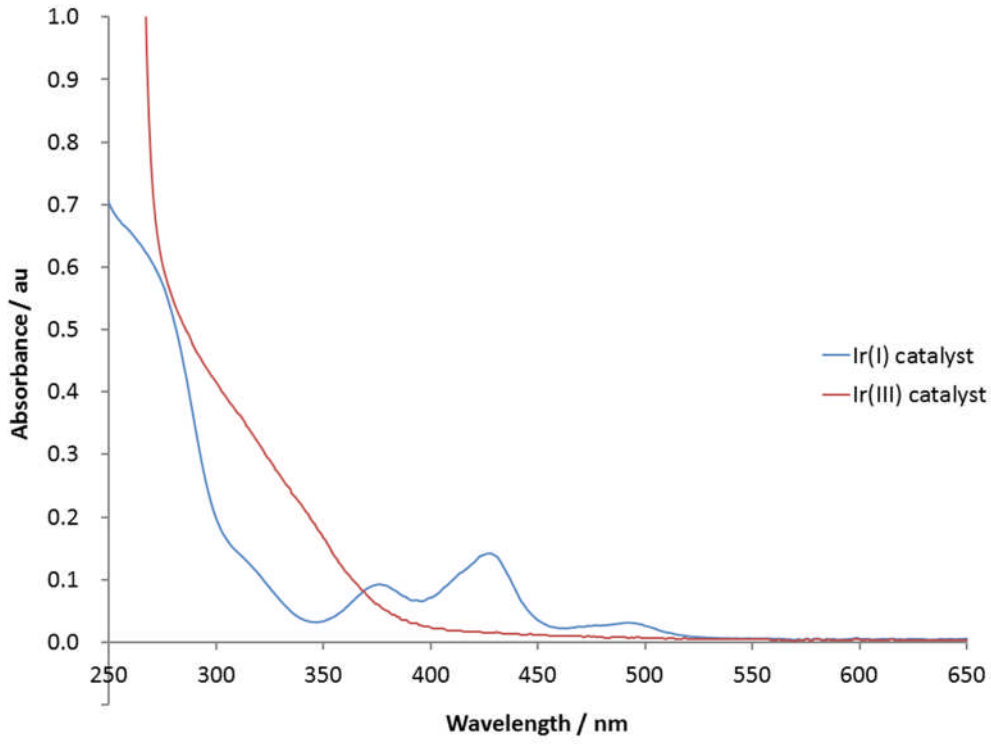

Figure S16. UV-vis spectra of 4 and [Ir(IMes)(H)₂(py)₃]Cl in methanol

IR data

The overlay IR spectra of **L_1HBr, 1** and **3** in Figure S17 shows that only the free carbene contains an O-H bending mode whilst the silver and iridium complexes do not have this signal, demonstrating that the phenolate remains bound to the metal centre.

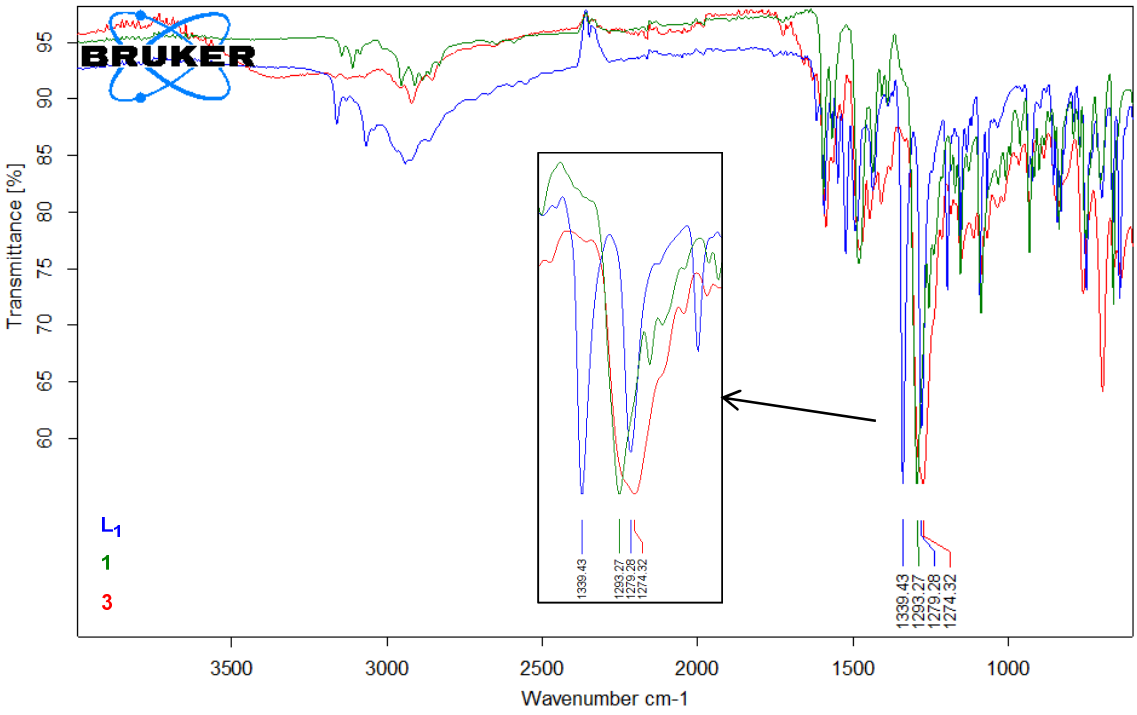

Figure S17. Comparison of the IR spectra of L_1HBr, 1 and 3

Lineshape analysis of the hydride exchange using Topspin DNMR program

At 298 K, in CD_2Cl_2 two hydrides signals for **3** are present at δ -28.8 and -21.4. On cooling, these two hydride resonances split and another pair of hydride signals evolve, so that the major isomer appears at δ -21.35 and -28.88 and the minor isomer appears at δ -22.68 and -29.02. This is due to a conformational isomer because of the seven-membered metallocycle which gives rise to an endo and exo seven-membered ring. This behaviour is illustrated in Figure S18.

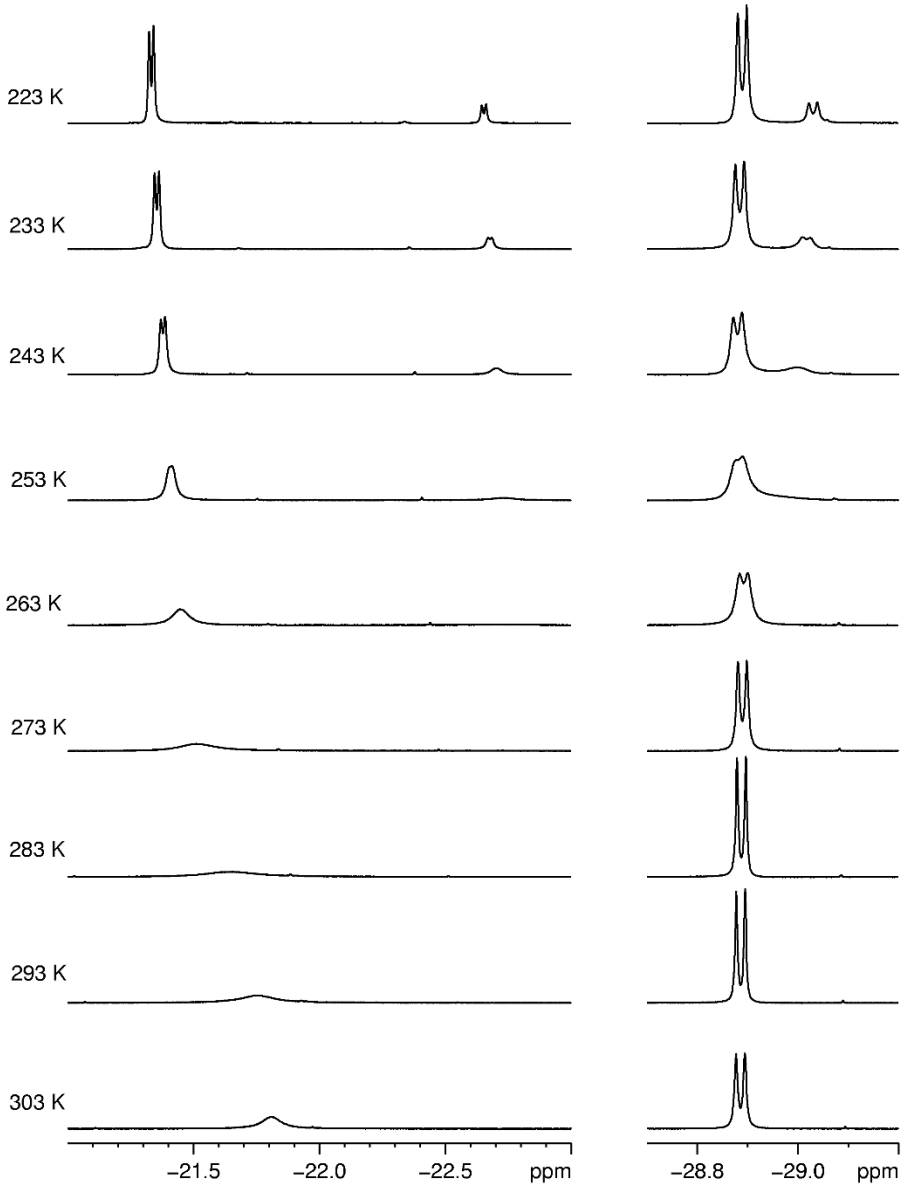

Figure S18. ^{1}H NMR spectra showing conformer separation upon decreasing temperature from 303 K to 223 K

The dynamic behaviour of **3** has been probed. EXSY experiments at 233 K enabled rates of exchange to be calculated between H_A (major isomer) and $H_{A'}$ (minor isomer). At 233K, the two sets of hydride resonances appear at δ -21.35 (H_A) and -29.88 (H_B), and at δ -22.68 ($H_{A'}$) and -29.02 ($H_{B'}$) with J_{AB} and $J_{A'B'}$ being 8.9 and 7.3 Hz respectively. The exchange rates could not be calculated for the exchange between H_B and $H_{B'}$ because the chemical shift difference between the two hydride peaks was too small. Using EXSY experiments, the exchange rate for conversion of H_A into $H_{A'}$ was calculated to be

4.00 ± 0.08 s^{-1} and the exchange rate for conversion of $H_{A'}$ into H_A was calculated to be 19.83 ± 0.33 s^{-1}. Table S14 and Figures S19 and S20 show the data for this exchange.

Table S14. Data for percentage conversion between each isomer when selectively exciting each hydride

Selective irradiation	**δ -21.35**		**δ -22.68**	
Mixing time / sec	**[H_A] / %**	**[$H_{A'}$] / %**	**[H_A] / %**	**[$H_{A'}$] / %**
0.005	97.91	2.10	90.37	9.63
0.010	96.19	3.81	82.90	17.10
0.050	88.42	11.58	43.77	56.23
0.070	86.38	13.62	33.73	66.27
0.100	85.01	14.99	26.70	73.30
0.150	83.97	16.03	22.60	77.40
0.200	83.76	16.24	21.21	78.79
0.250	83.54	16.46	20.76	79.24
0.300	83.57	16.43	20.42	79.58
0.350	83.59	16.41	20.75	79.25

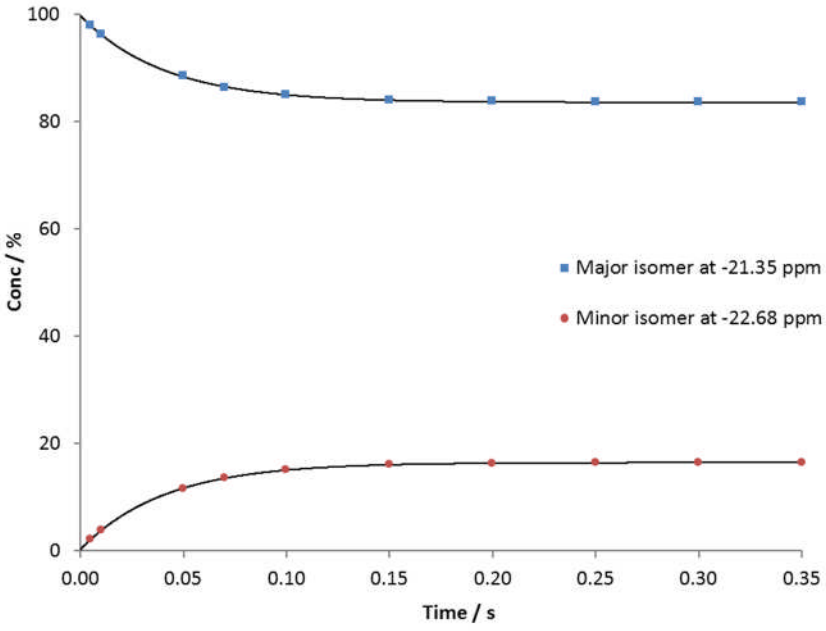

Figure S19. Conversion from H_A to $H_{A'}$ on selective excitation of H_A

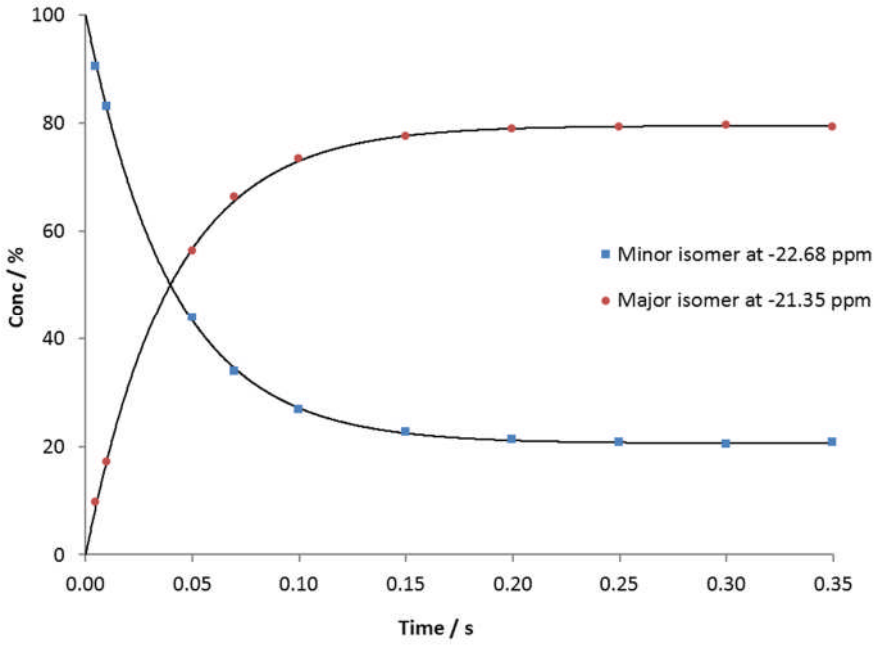

Figure S20. Conversion from $H_{A'}$ to H_A on selective excitation of $H_{A'}$

Using lineshape analysis the rate of exchange between each conformer can be estimated. Fitting each spectrum to the four lowest temperatures within the range studied, enabled the determination of rate constants at each temperature and an estimate of the activation energy using the Arrhenius equation and the Eyring-Polanyi equation as described before. Table S15 shows the simulated exchange rate values obtained, with the corresponding Arrhenius and Eyring-Polanyi plots in Figures S21 and S22 and the activation parameters summarized in Table S16.

H_A = δ -21.35

$H_{A'}$ = δ -22.68

H_B = δ -28.88

$H_{B'}$ = δ -29.02

Lineshape analysis on the exchanging hydrides at 223, 233 and 243 K proved possible when setting H_A and $H_{A'}$ to be exchanging and H_B and $H_{B'}$ to be exchanging. This generated spectra with a 96 % agreement level (data set A). When trying to simulate the data for the spectrum at 253 K the simulation program could not produce an accurate spectrum at 96 % agreement due to coalescence of the hydride peaks at δ ~-29.0. When these hydrides were set to be exchanging (data set B), the highest value that was obtained was ~85 %. If these two overlapping hydrides were set to not be exchanging (data set C) then a 96 % agreement level was reached.

Table S15. Simulated rate constants at the four lowest temperatures for each data set for hydride exchange

Temperature / K	Simulated rate for data set A / s^{-1}	Simulated rate for data set B / s^{-1}	Simulated rate for data set C / s^{-1}
223	0.64 ± 0.03	0.64 ± 0.03	0.64 ± 0.03
233	2.27 ± 0.09	2.27 ± 0.09	2.27 ± 0.09
243	5.59 ± 0.22	5.59 ± 0.22	5.59 ± 0.22
253	-	15.72 ± 2.36	11.47 ± 0.46

Data sets:

A: 96 % agreement level for each hydride for the lowest 3 temperatures

B: 96 % agreement level for 223, 233 and 243 K and 85 % for 253 K (δ -29 hydrides set to be exchanging)

C: 96 % agreement level for all temperatures (δ -29 hydrides set to not be exchanging)

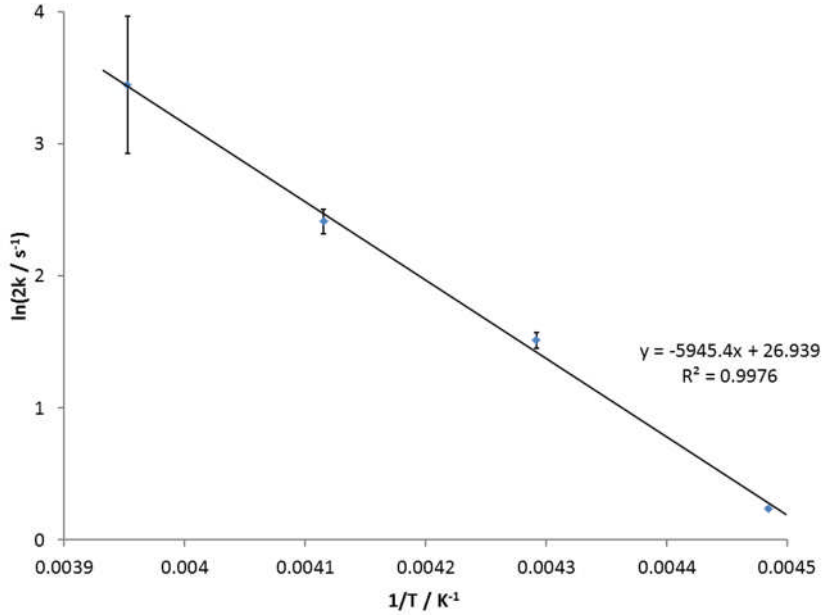

Figure S21. Arrhenius plot of the simulated hydride exchange rates using data set B

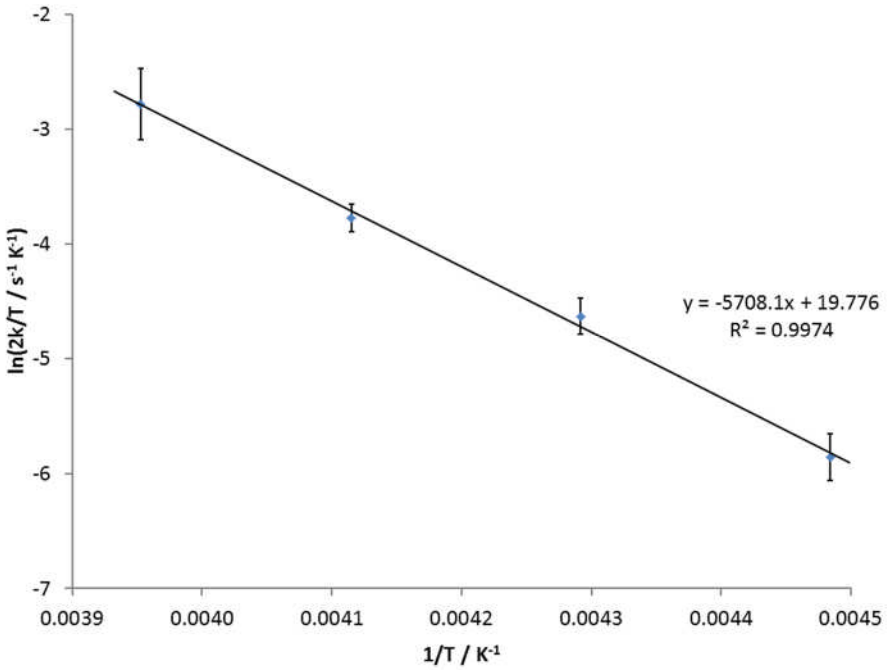

Figure S22. Eyring-Polanyi plot of the simulated hydride exchange rates using data set B

Table S16. Summary of activation parameters for the simulated data for the hydride exchange

Equation used	**Data set**	**Activation energy (E_a/$\Delta H^{\ddagger}$) / kJ mol^{-1}**	**Graph R^2 value**	**Activation entropy ($\Delta S^{\ddagger}$) / J K^{-1} mol^{-1}**	**ΔG (300 K) / J mol^{-1}**
Arrhenius	A	49.1 ± 7.3	0.9946	-	-
	B	49.4 ± 1.8	0.9976	-	-
	C	45.1 ± 5.8	0.9914	-	-
Eyring-Polanyi	A	47.2 ± 7.3	0.9940	-28.7 ± 31.5	55.8 ± 0.50
	B	47.5 ± 1.8	0.9974	-27.4 ± 7.5	55.7 ± 0.65
	C	43.1 ± 5.9	0.9904	-46.2 ± 24.5	57.0 ± 1.1

5. Exchange properties of 3 relating to SABRE

In order to explore the ligand exchange characteristics of **3** it is necessary to complete a series of variable temperature and concentration studies to explore the mechanism of these exchange pathways. We first consider pyridine and H_2 exchange at 298 K before examining the effect of increasing pyridine concentration in CD_2Cl_2. When changing to methanol an additional H-D exchange process is observed and as a consequence both H_2 loss and pyridine exchange are followed in MeOH-d_3. A variable temperature study is also conducted to determine appropriate activation parameters. This kinetic analysis is followed by an extension to examine the effect of increasing pyridine concentration in methanol. These results are detailed in Figures S23 – S32 and Tables S17 – S26.

Pyridine exchange rates in CD_2Cl_2

Exchange rates between free pyridine and both the axial and equatorial pyridine sites were calculated in CD_2Cl_2 at 298 K. It was found that only the equatorial pyridine exchanged with free pyridine on the NMR timescale. The experimental dissociation rate constant was calculated to be 0.28 ± 0.03 s^{1} for a sample containing a 25-fold excess of pyridine compared to catalyst.

Table S17. Data for percentage incorporation of free pyridine into bound pyridine

Mixing time / sec	[Equatorial bound pyridine] / %	[Free pyridine] / %
0.05	98.45	1.55
0.10	96.98	3.02
0.20	94.76	5.24
0.30	93.19	6.81
0.40	92.19	7.81
0.50	91.40	8.60
0.60	89.97	10.03
0.70	89.15	10.85
0.80	88.77	11.23
0.90	88.12	11.88

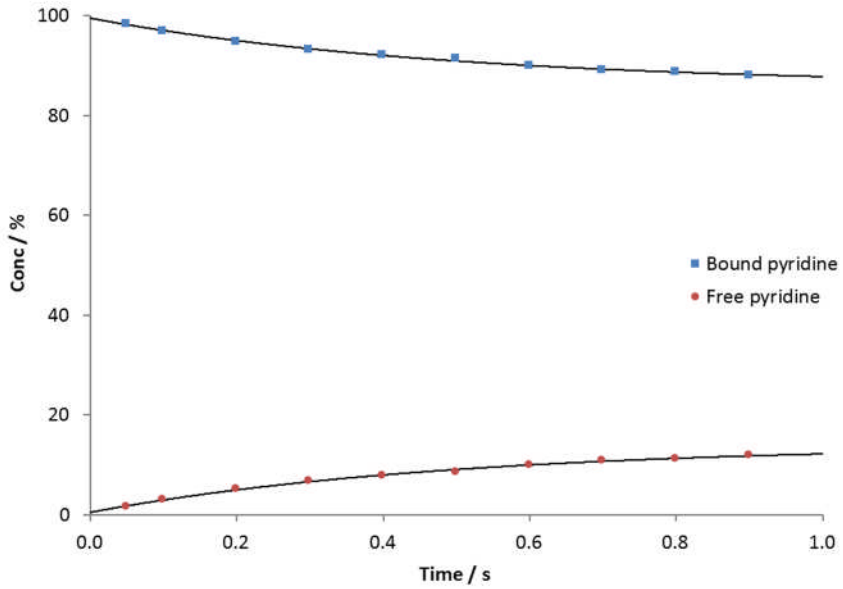

Figure S23. Equatorial and free pyridine exchange for the bound pyridine at δ 8.31 at 298 K in 3

Hydride-hydrogen exchange at 298 K in CD_2Cl_2

At 298 K the two hydrides undergo exchange. The hydride signal at δ -28.9 was selectively excited although the hydride signal at δ -21.8 was much broader so was not able to be selectively excited. The data shown is for a sample containing a 25-fold excess of pyridine compared to catalyst.

Table S18. Data for percentage incorporation from the hydride at δ -28.9 into the hydride at δ -21.8 and free H_2

Mixing time / sec	[δ -28.9 hydride (A)] / %	[δ -21.8 hydride (B)] / %	[H_2 in solution (C)] / %
0.05	98.08	1.75	0.17
0.10	93.78	5.92	0.30
0.20	86.19	12.84	0.98
0.30	78.83	19.53	1.64
0.40	73.71	23.97	2.32
0.50	69.84	27.17	2.99
0.60	64.80	31.16	4.04
0.70	61.63	33.77	4.59
0.80	61.13	33.01	5.85
0.90	58.41	35.03	6.56

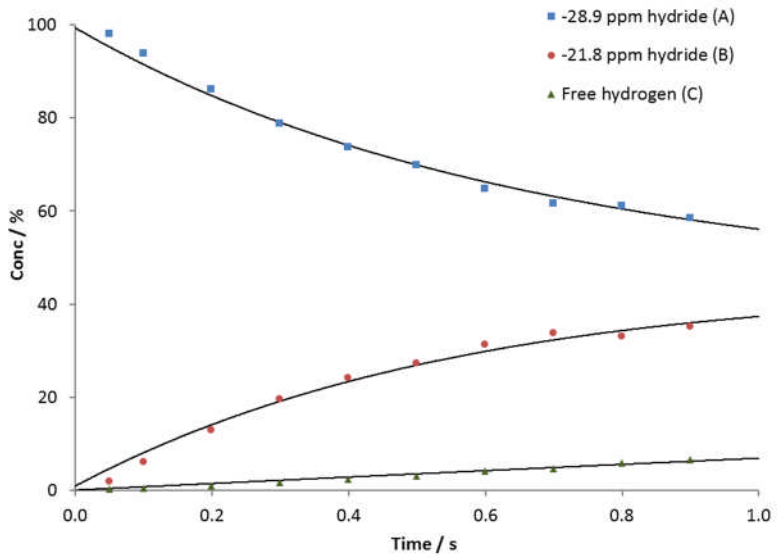

Figure S24. Hydride and hydrogen exchange from the hydride at δ -28.9 at 298 K in 3

Using this data, exchange rates for the different processes can be calculated. The hydrides were shown to exchange with each other at a rate of 0.79 ± 0.02 s^{-1} and the dissociative rate from each hydride to hydrogen was calculated to be 0.071 ± 0.003 s^{-1}. In CD_2Cl_2, the rate of pyridine exchange was found to be independent of pyridine concentration whereas the rate constant for hydride loss decreased upon addition of pyridine. This suggests that the process follows a dissociative mechanism in dichloromethane.

Table S19. Exchange rates and normalised exchange rates for pyridine and hydride loss

No. of eq. of py by NMR ratio	Rate of py loss / k / s^{-1}	Normalised rate of py loss	Rate of H loss / k / s^{-1}	Normalised rate of H loss
15	0.28 ± 0.03	0.9032	0.078 ± 0.003	1.0000
25	0.28 ± 0.03	0.9032	0.071 ± 0.003	0.9103
30	0.31 ± 0.01	1.0000	0.053 ± 0.002	0.6795
50	0.28 ± 0.03	0.9032	0.042 ± 0.002	0.5385

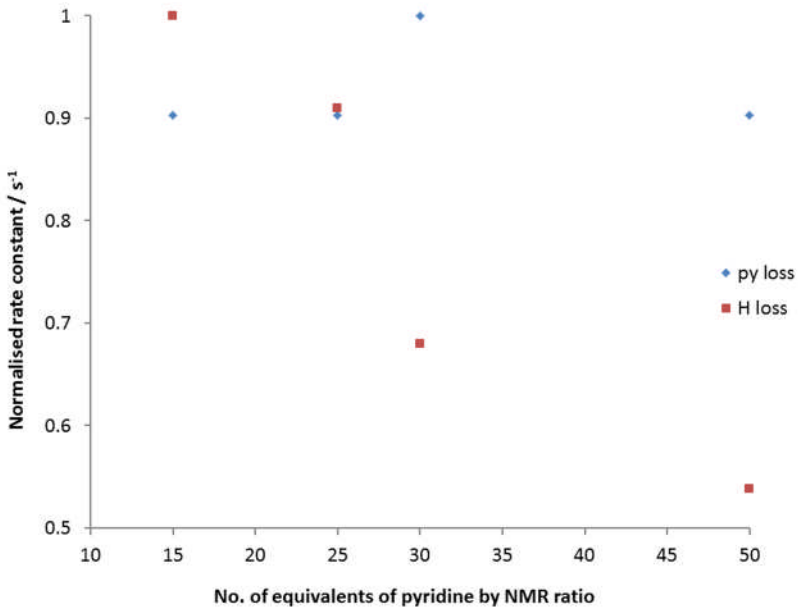

Figure S25. The normalised rates of pyridine and hydride loss in relation to the number of equivalents of pyridine added, calculated by NMR ratio

Hydride-Deuterium Exchange rates in MeOD-d_4

At 243 K, the two hydrides of the major conformer are easily visible as two doublets. However, at 243 K, **3** in MeOD-d_4 does not seem to undergo H-D exchange on the NMR timescale. An equilibrium is maintained at approximately 13 % H-D complex and 86 % H-H complex where deuteration could have occurred directly after addition of hydrogen to the sample before the sample was cooled down. At temperatures above 243 K, the hydride signal at δ -24.7 becomes very broad and so any exchange process is not observable. At 270 K, H-D exchange of the hydride signal at δ -29.2 occurs. The values were calculated by using the integral areas of the two signals and normalising their total value to 100 %. The H-D exchange rate was calculated to be 4.23×10^{-5} s^{-1}. This shows that the exchange process is slow at low temperature. As the temperature was increased to 298 K the H-D exchange process became much faster. After 10 minutes in the spectrometer ~ 34 % of the sample was deuterated, therefore in order to calculate a rate for the exchange process, it was assumed that initially the concentration of deuterated sample was 0 %. Using this data the rate of exchange was calculated to be 8.19×10^{-4} s^{-1} which is ~ 20 times faster than the exchange process at 270 K and therefore for every increase by 10 degrees, the rate increases by nearly 7 times.

Table S20. Data for percentage incorporation of deuterium into the hydride at δ -29 at 270 K

Time / min	[H-H] / %	[H-D] / %
0	92.34	7.66
10	92.82	7.18
20	90.63	9.37
30	88.30	11.70
40	87.38	12.62
50	86.13	13.87
60	82.67	17.33
70	82.15	17.85
80	80.50	19.50
90	77.70	22.30
100	76.49	23.51
110	76.37	23.63
120	75.03	24.97
130	74.29	25.71
140	72.60	27.40
150	72.82	27.18

160	70.69	29.31
170	69.80	30.20
180	70.15	29.85
190	68.07	31.93
200	67.16	32.84
210	67.37	32.63
220	66.81	33.19
230	65.01	34.99
240	63.37	36.63

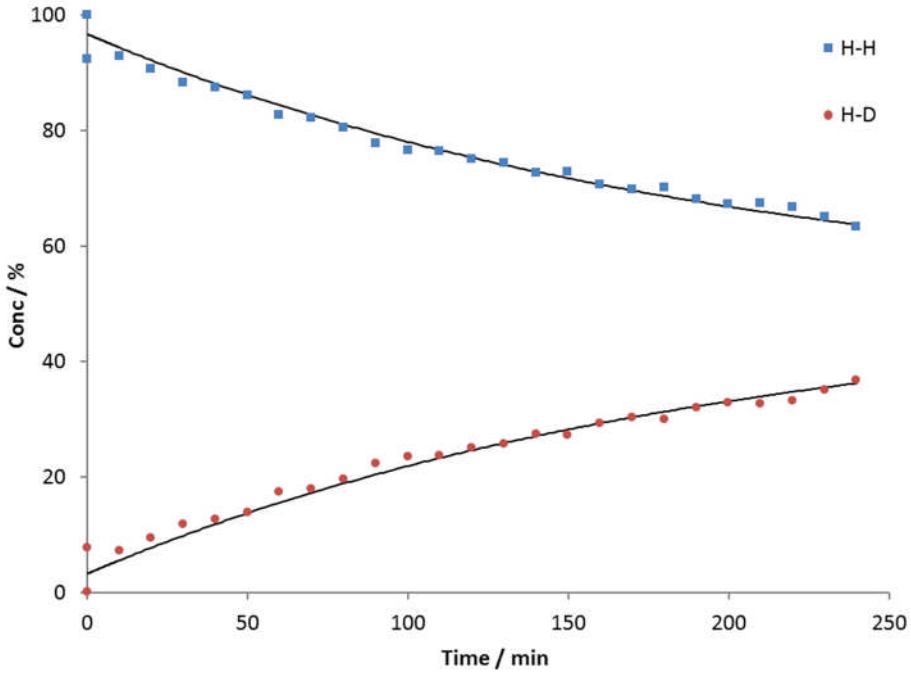

Figure S26. Hydride and Deuterium exchange for hydride at δ -29 at 270 K in 3

Table S21. Data for percentage incorporation of deuterium into the hydride at δ -29 at 298 K

Time / min	[H-H] / %	[H-D] / %
0	100.00	0.00
10	66.16	33.84
20	45.66	54.34
30	43.70	56.30
40	39.16	60.84
50	35.10	64.90
60	33.93	66.07

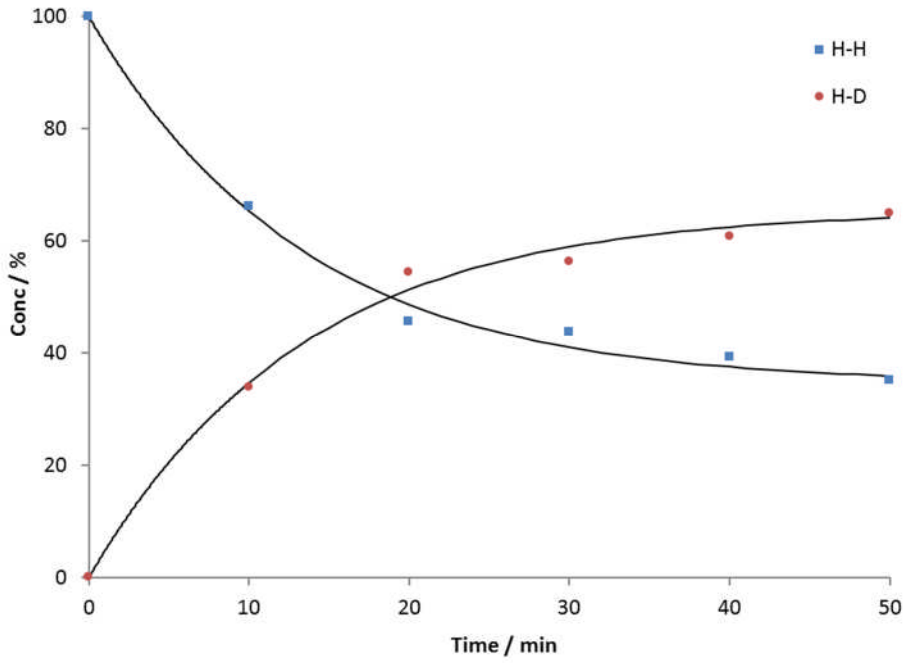

Figure S27. Hydride and Deuterium exchange for hydride at δ -29 at 298 K in 3

Pyridine exchange at 298 K in MeOH-d_3 (10 eq. of pyridine)

A sample of **3** in MeOH-d_3 containing 10 equivalents of pyridine was used to calculate exchange rates of the active catalyst because no deuteration effects occurred. It was again found that only the equatorial pyridine exchanged with free pyridine on the NMR timescale and that the axial pyridine did not exchange. The rate of dissociation was calculated to be 0.79 ± 0.04 s^{-1}.

Table S22. Data for percentage incorporation of free pyridine into bound pyridine

Mixing time / sec	[Equatorial bound pyridine] / %	[Free pyridine] / %
0.05	96.01	3.99
0.10	92.55	7.45
0.20	85.48	14.52
0.30	79.91	20.10
0.40	75.00	25.00
0.50	69.01	30.99
0.60	65.31	34.69
0.70	60.61	39.39
0.80	56.97	43.04
0.90	55.30	44.70

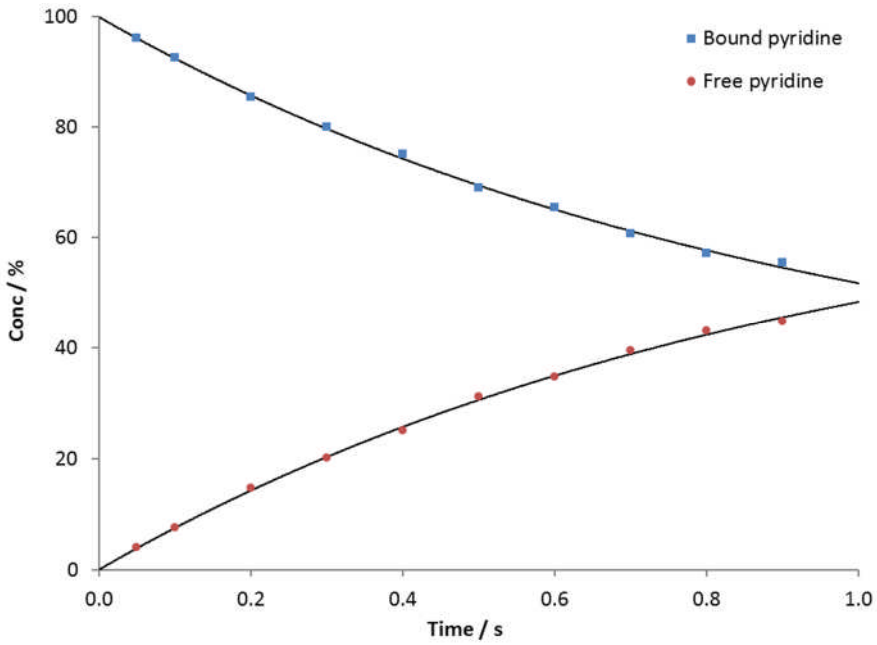

Figure S28. Equatorial and free pyridine exchange for the bound pyridine at δ 8.21 at 298 K in 3 in MeOH-d_3

Hydride-hydrogen exchange at 298 K in MeOH-d_3 (10 eq. of pyridine)

In MeOH-d_3, when the hydride at δ -29.2 was selectively irradiated via EXSY experiments the percentage proportion of each hydride and hydrogen could be calculated after ten different mixing times from 0.05 s to 0.90 s. The rate of exchange with the other hydride at δ -21.6 was calculated to be 2.04 ± 0.06 s^{-1}. The dissociative rate from each hydride to hydrogen was calculated to be 0.33 ± 0.02 s^{-1}.

Table S23. Data for percentage incorporation from the hydride at δ -29.2 into the hydride at δ -21.6 and free H_2

Mixing time / sec	[δ -29.2 hydride (A)] / %	[δ -21.6 hydride (B)] / %	[H_2 in solution (C)] / %
0.05	89.68	10.25	0.07
0.10	79.27	18.27	2.46
0.20	72.51	23.16	4.33
0.30	66.46	28.05	5.49
0.40	62.04	30.57	7.39
0.50	57.85	32.97	9.18
0.60	54.85	34.03	11.12
0.70	52.69	34.27	13.04
0.80	50.95	35.82	13.23
0.90	46.59	34.01	19.40

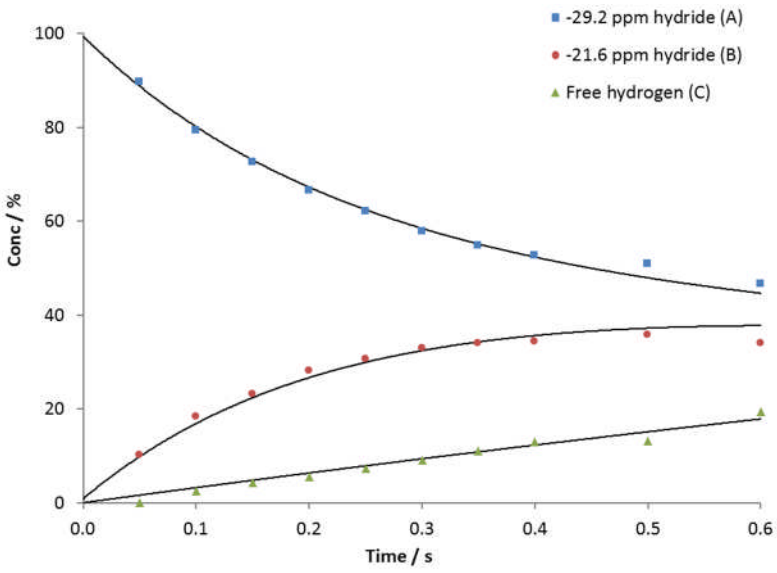

Figure S29. Hydride and hydrogen exchange from the hydride at δ -29.2 at 298 K in 3 in MeOH-d_3

Exchange rates for pyridine and hydride at 294 K in MeOH-d_3

To determine the mechanism for exchange in MeOH-d_3 a sample of **1** in MeOH-d_3 and activated with pyridine and hydrogen was used. At each concentration of pyridine, the use of EXSY experiments enabled the percentage proportions of bound vs free pyridine and each hydride vs hydrogen to be calculated. Therefore the pyridine and hydride exchange rates could be measured at each concentration of pyridine. The experimentally determined rate constant for pyridine dissociation was found to average at 0.78 ± 0.03 s^{-1} and the rate constants for hydride loss averaged at 2.19 ± 0.07 s^{-1}. As the concentration of pyridine increased, the hydride dissociation loss decreased. This shows that the pathway follows a dissociative mechanism with pyridine loss occurring before hydride exchange.

Table S24. Rates of pyridine and hydride dissociation for 3 with increasing equivalents of pyridine

Pyridine equivalents by NMR ratio	Rate of pyridine dissociation / s^{-1}	Rate of hydride δ -29.2 dissociation / s^{-1}	Rate of hydride interconversion δ -29.2 to -21.6 / s^{-1}
6	0.83 ± 0.06	0.850 ± 0.110	2.02 ± 0.11
10	0.79 ± 0.04	0.330 ± 0.016	2.05 ± 0.06
15	0.78 ± 0.02	0.230 ± 0.013	2.44 ± 0.03
20	0.80 ± 0.02	0.160 ± 0.007	2.49 ± 0.07
25	0.76 ± 0.04	0.092 ± 0.002	2.06 ± 0.09
30	0.72 ± 0.01	0.072 ± 0.004	2.07 ± 0.08

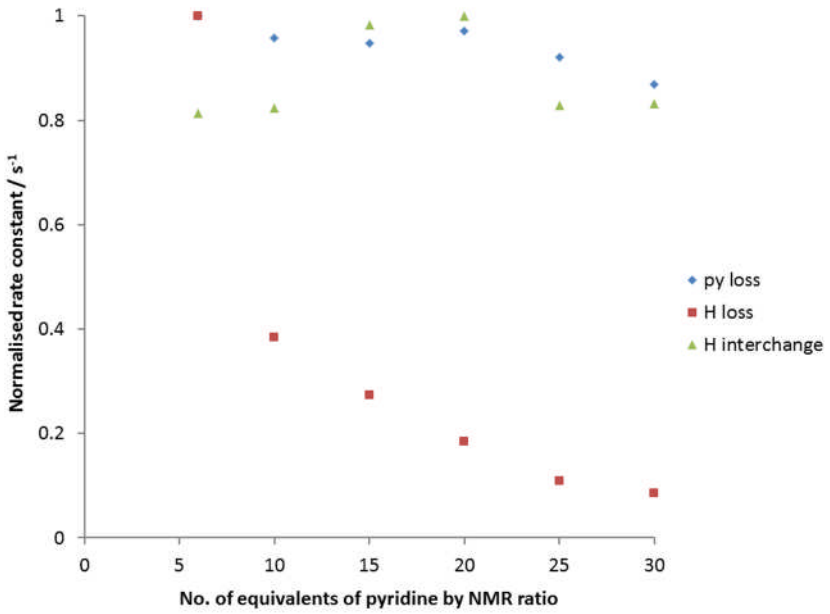

Figure S30. Normalised rates of pyridine dissociation, hydride dissociation and hydride interchange for a sample containing increasing amounts of pyridine as determined by ^1H NMR

Exchange rates vs temperature in MeOH-d_3

The exchange rates of bound pyridine to free pyridine and hydride to hydrogen were measured at different temperatures in order to gain activation parameters and relate the exchange rates to observed enhancement levels. The use of EXSY experiments, selectively irradiating the equatorial bound pyridine and then selectively irradiating the hydride *trans* to the oxygen at δ -28.88, at temperatures from 278 K to 303 K gave increasing rate constants.

Table S25. Exchange rate data for pyridine dissociation and hydride dissociation at different temperatures in 3 in MeOH-d_3

T / K	Rate of pyridine dissociation / s^{-1}	Rate of hydride δ – 29.2 dissociation / s^{-1}	Rate of hydride interconversion δ -29.2 to -21.6 / s^{-1}
278	0.17 ± 0.02	0.09 ± 0.02	0.19 ± 0.02
283	0.29 ± 0.11	0.11 ± 0.01	0.52 ± 0.04
288	0.53 ± 0.04	0.19 ± 0.03	1.09 ± 0.11
293	0.83 ± 0.02	0.36 ± 0.03	1.84 ± 0.16
298	1.33 ± 0.23	0.54 ± 0.03	2.86 ± 0.18
303	2.52 ± 0.30	0.96 ± 0.06	3.59 ± 4.25

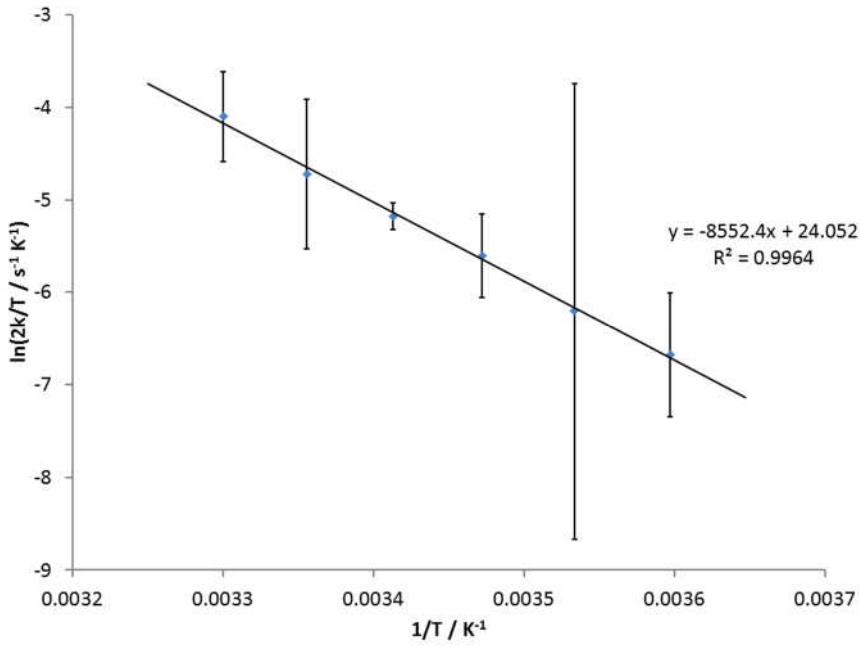

Figure S31. An Eyring-Polanyi plot for pyridine exchange at differing temperatures in 3 in MeOH-d_3

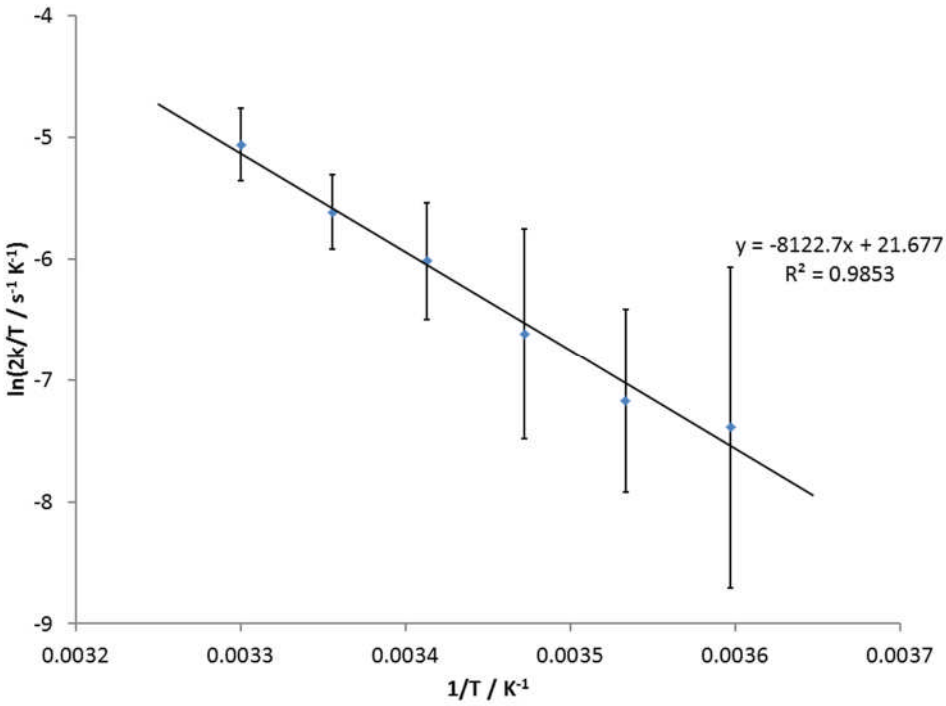

Figure S32. An Eyring-Polanyi plot for hydride-hydrogen exchange at differing temperatures in 3 in MeOH-d_3

Table S26. Activation parameters calculated from the Arrhenius and Eyring-Polanyi plots for pyridine dissociation and hydride dissociation in 3 in MeOH-d_3

	Pyridine				**Hydride**			
	E_a / ΔH / kJ mol^{-1}	**ΔS / J K^{-1}**	**R^2 value**	**ΔG (300 K) / kJ mol^{-1}**	**E_a / ΔH / kJ mol^{-1}**	**ΔS / J K^{-1}**	**R^2 value**	**ΔG (300 K) / kJ mol^{-1}**
Arrhenius equation	73.5 ± 3.3		0.9966		69.9 ± 7.3		0.9862	
Eyring-Polanyi equation	71.1 ± 3.3	2.4 ± 11.5	0.9964	70.4 ± 0.2	67.5 ± 7.3	-17.3 ± 24.7	0.9853	72.7 ± 0.2

6. Polarization transfer experiments

Polarization transfer experiments were conducted in either a Young's tube (Method A) or by using a polarizer as described elsewhere[4] (Method B).

Method A. Samples for polarization transfer experiments were conducted using a Young's NMR tube containing a solution of **1** or **4** (5 mol%), analyte (6.2 x 10^{-5} mol) in 0.6 ml of MeOD-d_4. The sample was degassed prior to the introduction of *p*-H_2 at a pressure of 3 bar. The sample was placed in a water bath of known temperature for 1 min before shaking in the desired magnetic field (using the fringe field of the magnet) for 10 s before being rapidly transported to the magnet for interrogation by NMR spectroscopy.

Method B. Samples polarized using the polarizer were achieved as follows. The polarization chamber was charged with either **1** or **4** (5 mol%) and the nitrogen heterocycle to be polarized (0.1 M) in MeOD-d_4 (3 ml). Parahydrogen was introduced to the solution via six inlet tubes at a pressure of 3 bar for 10 s. This solution was then transferred into the Bruker Avance III series 400 MHz spectrometer equipped with a TXO flow probe head (flow cell volume = 200 µl) for interrogation by NMR using helium as a flow gas. A single transient was recorded for the nucleus of interest. Once interrogated, the solution could be returned to a polarizing chamber and this process repeated as required. A coil surrounded the reaction chamber such that a magnetic field could be generated in the *z* direction. This coil was designed to produce static DC fields in the range of −150 to 150 x10^{-4} T. For field profiling five ^{1}H NMR spectra were collected at each point to ensure reproducibility.

Calculation of ^{1}H NMR enhancement factors

For calculation of the enhancement shown by the ^{1}H NMR signals the following formula was used:

$$E = \frac{S_{pol}}{S_{unpol}}$$

E = enhancement

S_{pol} = signal of the polarized sample

S_{unpol} = signal of the unpolarized (reference) sample

Experimentally, the reference spectra were acquired with the same sample that was used for the hyperpolarized measurement after it had fully relaxed (typically 5-10 minutes at high magnetic field). Reference and polarized spectra were collected using identical acquisition parameters, particularly the receiver gain. The raw integrals of the relevant resonances in the polarized and unpolarized spectra were used to determine the enhancement level.

Samples for polarization transfer experiments

Extensive investigations into the SABRE polarization of pyridine and nicotinamide, shown in Figure S33, by **1** have been conducted in MeOD-d_4 and appropriate spectra are detailed in Figures S34 – S44 for pyridine and Figures S45 – S57 for nicotinamide. These include typical results for proton and carbon polarization as a function of both ligand concentration and temperature as well as OPSY spectra. Analysis of the effect of solvent on pyridine polarization is also detailed in Figure S58 and Table S27.

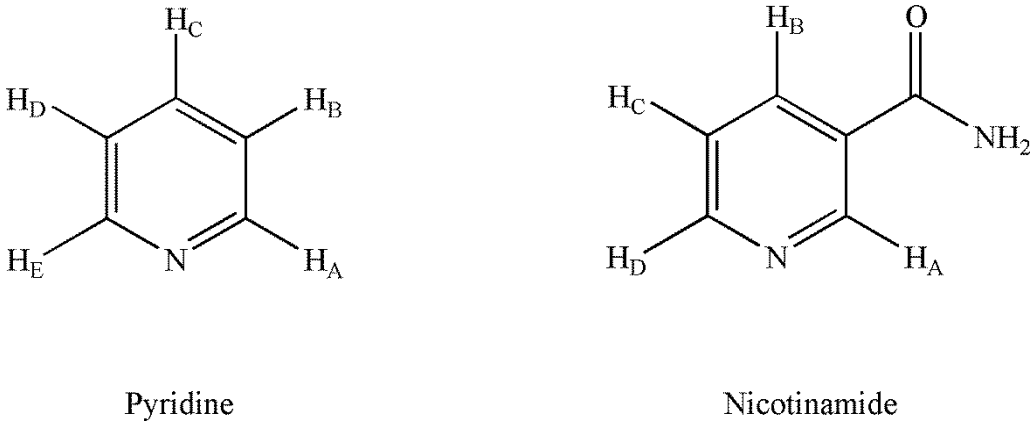

Figure S33. Analytes tested and their proton assignments

Polarization transfer to pyridine using 1 as a catalyst using method A

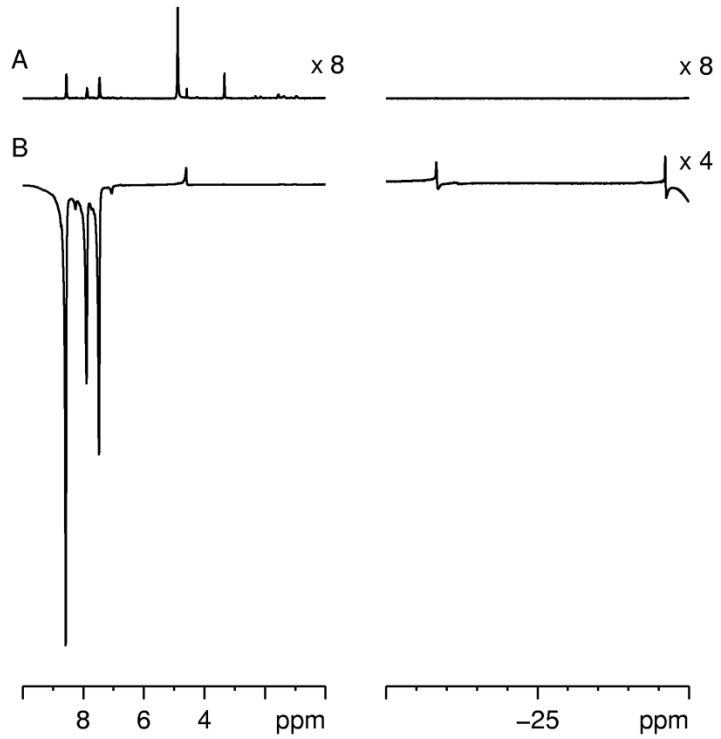

Figure S34. ^{1}H NMR spectra of a sample containing 0.1 M pyridine and 5 mol% 1 in MeOD-d_4 after; (A) thermal equilibrium at high field; and (B) polarization transfer from p-H_2 at 6.5 x10^{-3} T and 60 °C

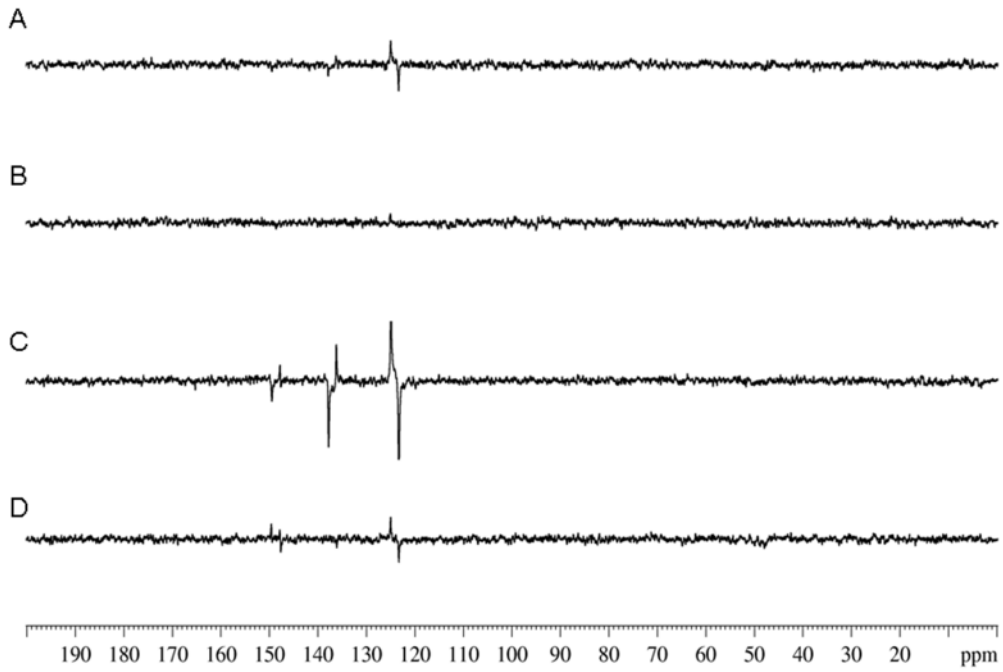

Figure S35. *^{13}C NMR spectra of a sample containing 0.1 M pyridine and 5 mol% 1 in MeOD-d_4 after polarization transfer at; (A) 0°C and 6.5 x10^{-3} T; (B) 0°C and 2 x10^{-4} T; (C) 60°C and 6.5 x10^{-3} T; and (D) 60°C and 2 x10^{-4} T*

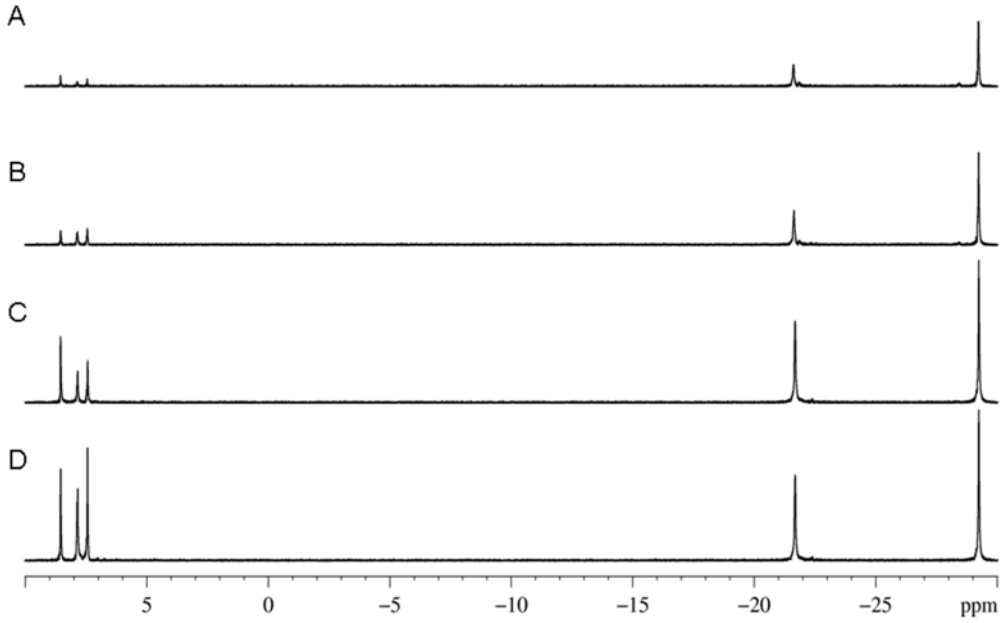

Figure S36. *^{1}H OPSY-dq NMR spectra of a sample containing 0.1 M pyridine and 5 mol% 1 in MeOD-d_4 after polarization transfer at; (A) 0°C and 6.5 x10^{-3} T; (B) 0°C and 2 x10^{-4} T; (C) 61°C and 6.5 x10^{-3} T; and (D) 61°C and 2 x10^{-4} T*

Polarization transfer to pyridine using 1 as a catalyst using method B

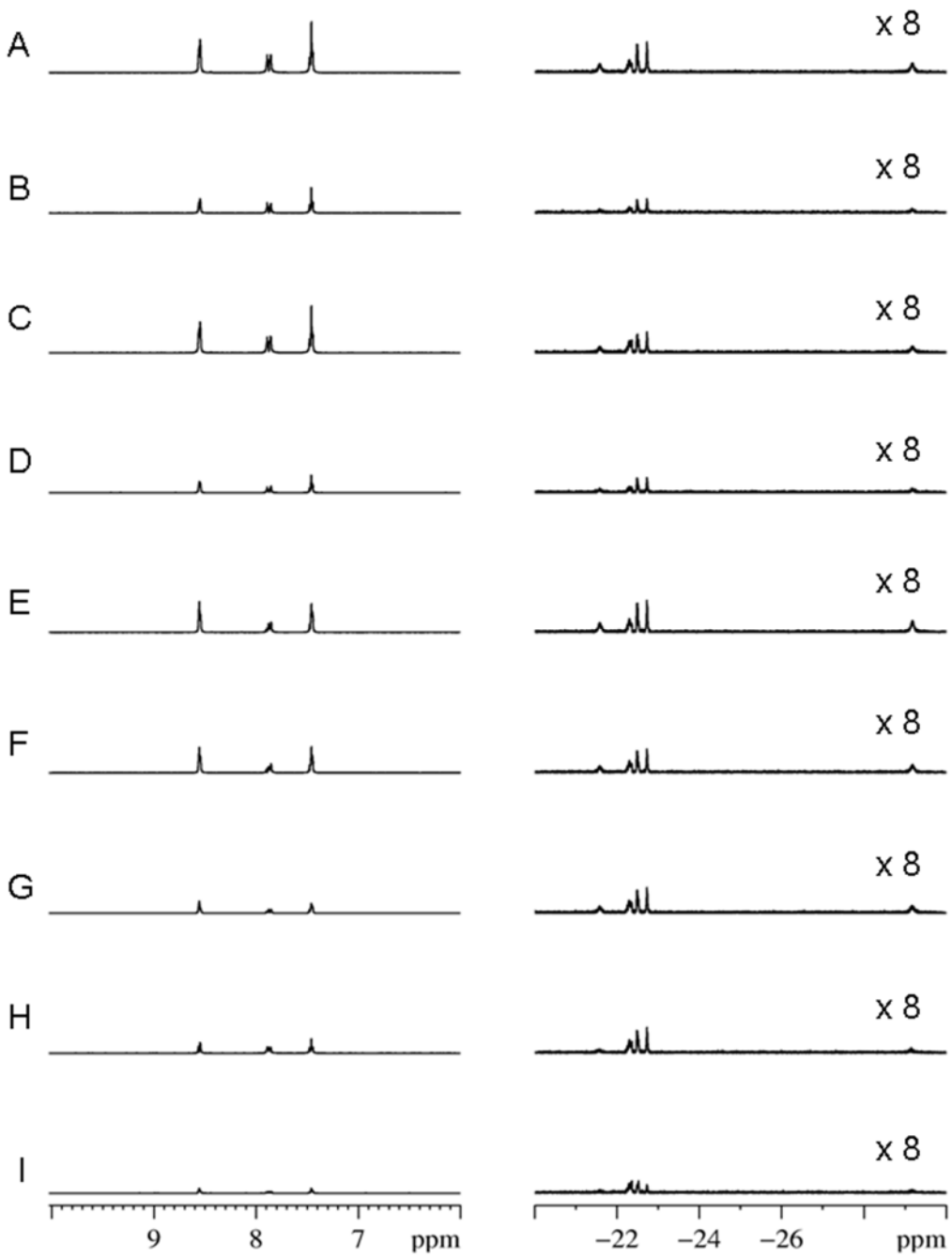

Figure S37. *^{1}H OPSY-dq NMR spectra of a sample containing 0.1 M pyridine and 5 mol% 1 in MeOD-d_4 after polarization transfer at RT and; (A) 2.5 x10^{-3} T; (B) 0 x10^{-4} T; (C) −2.5 x10^{-3} T; (D) −5 x10^{-3} T; (E) −6.5 x10^{-3} T; (F) 7.5 x10^{-3} T; (G) −1 x10^{-2} T; (H) −1.25 x10^{-2} T; (I) −1.5 x10^{-2} T*

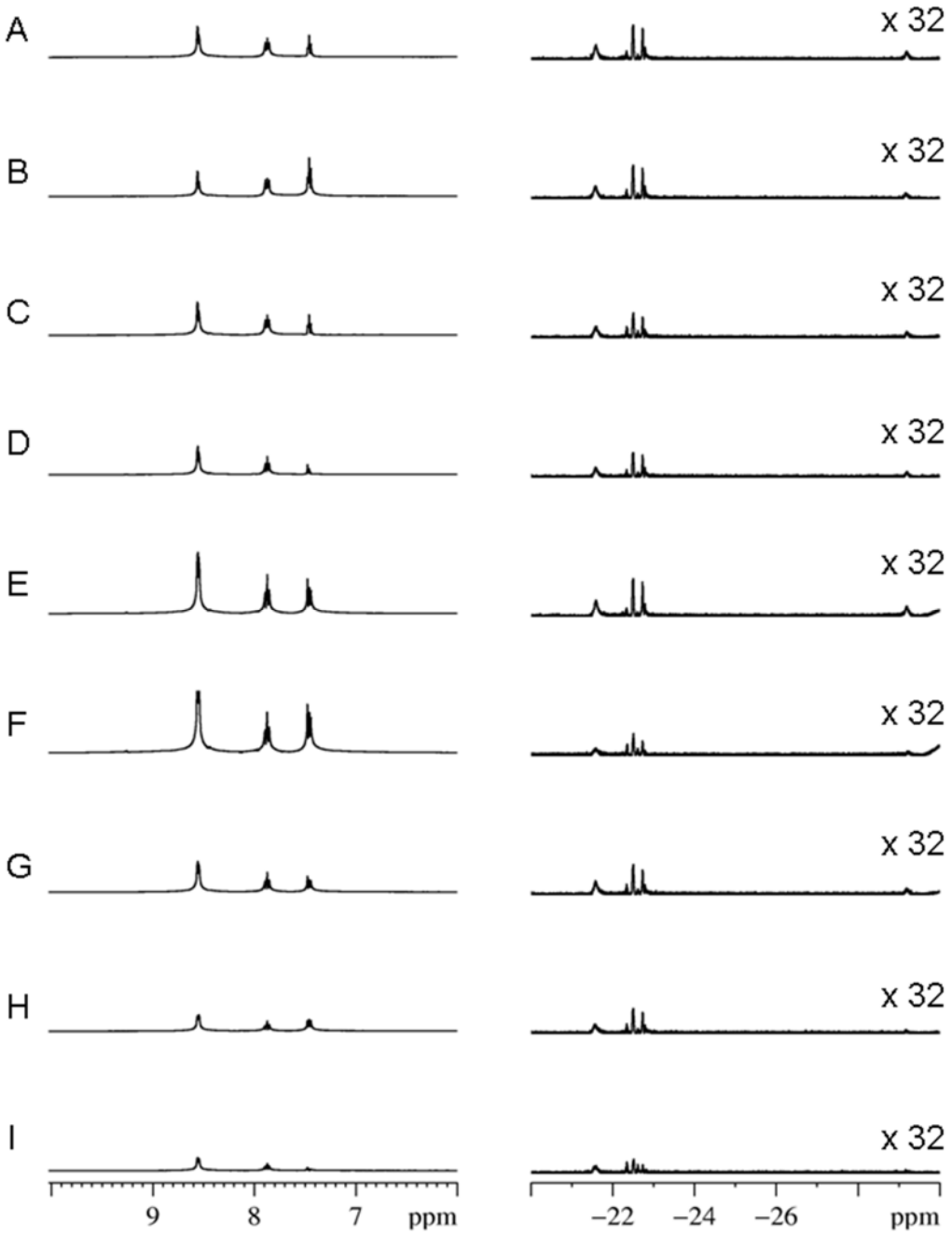

Figure S38. *^{1}H OPSY-zq NMR spectra of a sample containing 0.1 M pyridine and 5 mol% 1 in MeOD-d_4 after polarization transfer at RT and; (A) 2.5 x10^{-3} T; (B) 0 x10^{-4} T; (C) −2.5 x10^{-3} T; (D) −5 x10^{-3} T; (E) −6.5 x10^{-3} T; (F) 7.5 x10^{-3} T; (G) −1 x10^{-2} T; (H) −1.25 x10^{-2} T; (I) −1.5 x10^{-2} T*

Influence of temperature on polarization transfer to pyridine using 1 as a catalyst using method A

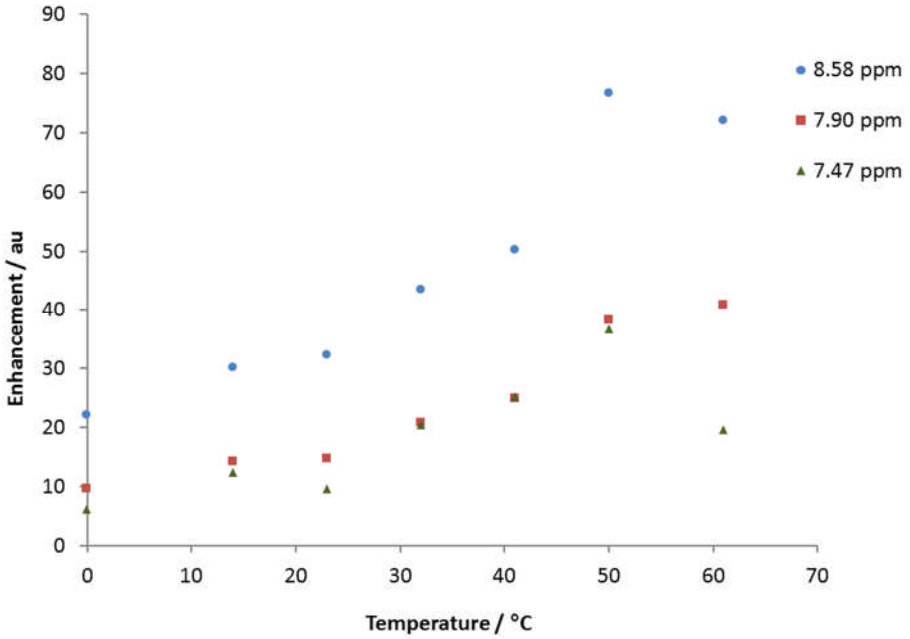

Figure S39. Enhancement observed for each type of ^{1}H resonance (H_A and H_E●, H_C ■ and H_B and H_D▲) of pyridine after polarization transfer from p-H_2 using 1 at 2 x10^{-4} T

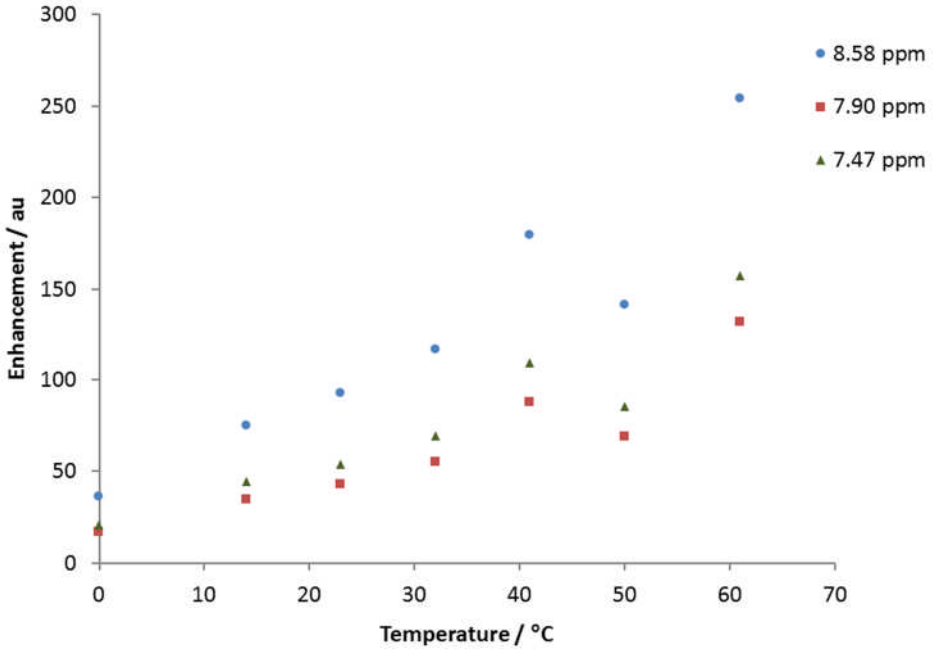

Figure S40. Enhancement observed for each type of ^{1}H resonance (H_A and H_E●, H_C ■ and H_B and H_D▲) of pyridine after polarization transfer from p-H_2 using 1 at 6.5 x10^{-3} T

Influence of temperature on polarization transfer to pyridine using 4 as a catalyst using method A

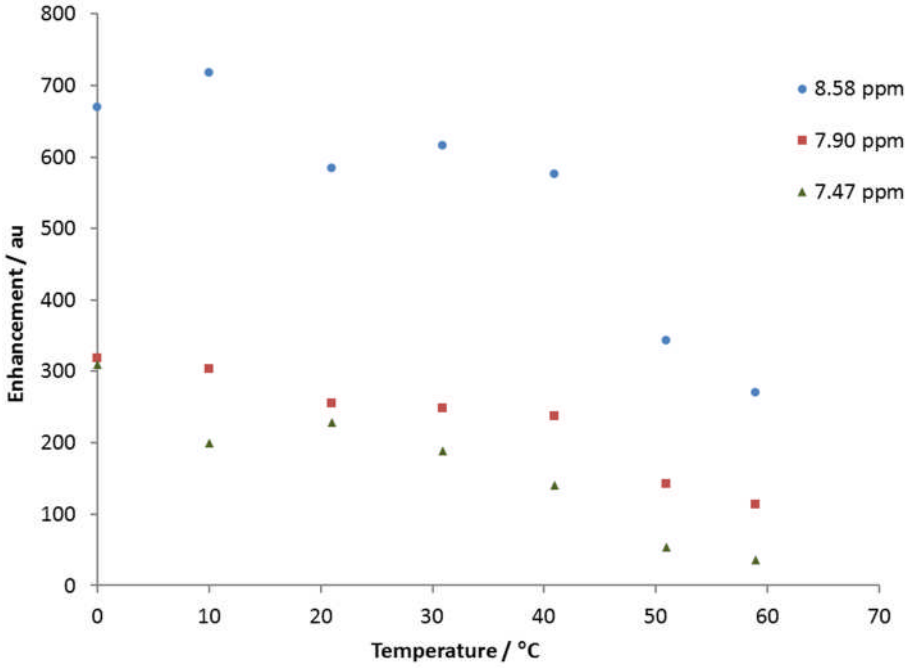

Figure S41. Enhancement observed for each type of ^{1}H resonance (H_A and H_E●, H_C ■ and H_B and H_D▲) of pyridine after polarization transfer from p-H_2 using 4 at 2 x10^{-4} T

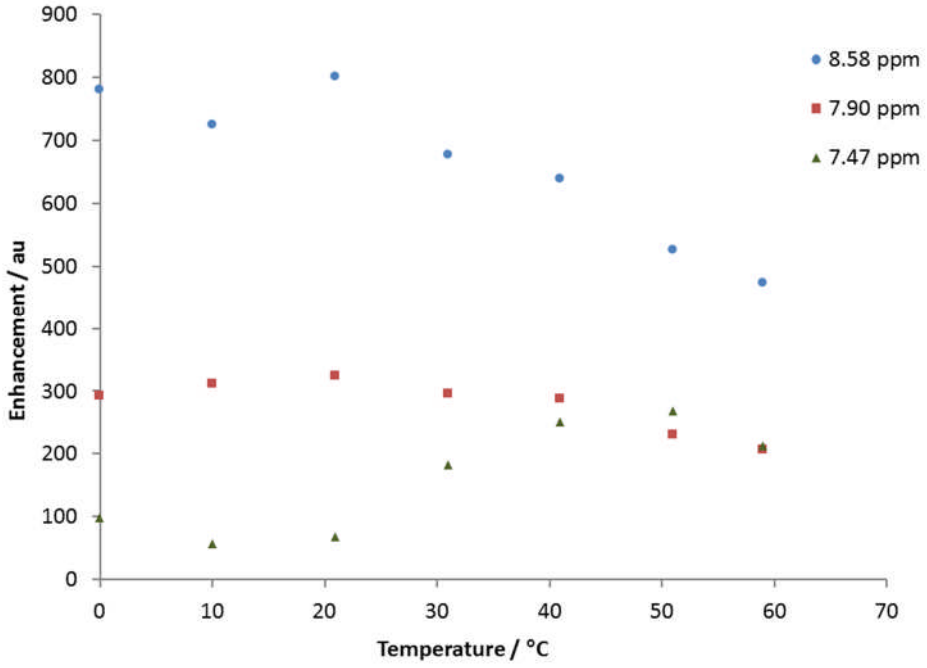

Figure S42. Enhancement observed for each type of ^{1}H resonance (H_A and H_E●, H_C ■ and H_B and H_D▲) of pyridine after polarization transfer from p-H_2 using 4 at 6.5 x10^{-3} T

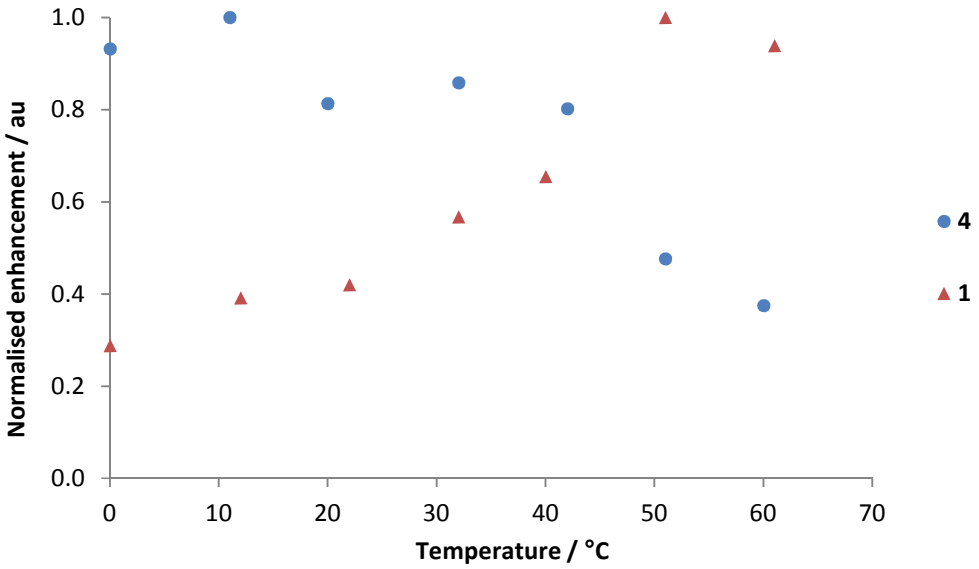

Figure S43. Normalised enhancement of the $H_{A/E}$ ^1H NMR resonance of pyridine after polarization transfer using p-H_2 at 2 x 10^{-4} T; one containing pyridine (0.1M) and 4 (2 mg) in deuterated methanol (0.6 ml) and one containing pyridine (0.1M) and 1 (2 mg) in deuterated methanol (0.6 ml)

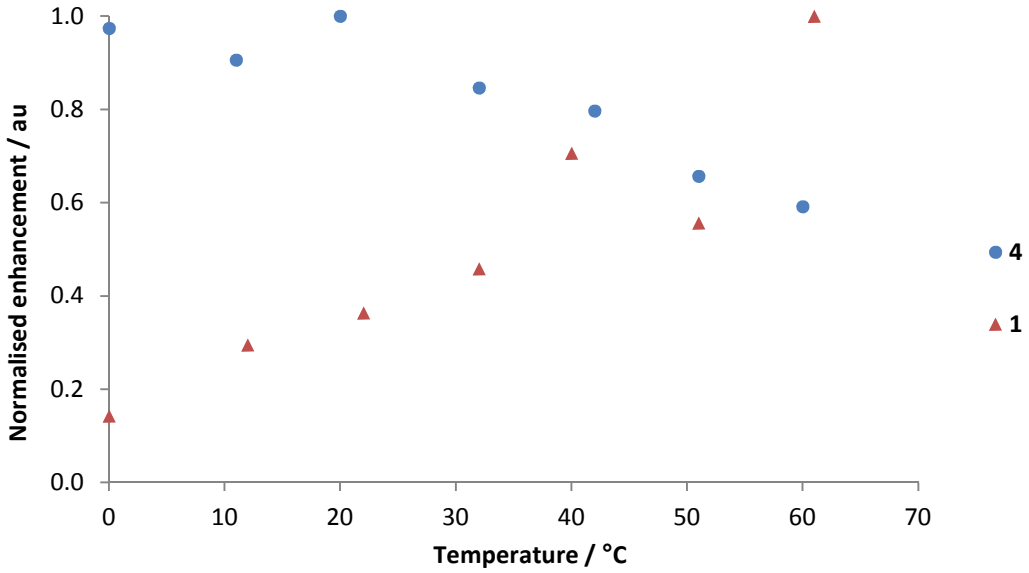

Figure S44. Normalised enhancement of the $H_{A/E}$ ^1H NMR resonance of pyridine after polarization transfer using p-H_2 at 6.5 x 10^{-3} T; one containing pyridine (0.1M) and 4 (2 mg) in deuterated methanol (0.6 ml) and one containing pyridine (0.1M) and 1 (2 mg) in deuterated methanol (0.6 ml)

Polarization transfer to nicotinamide using 1 as a catalyst using method A

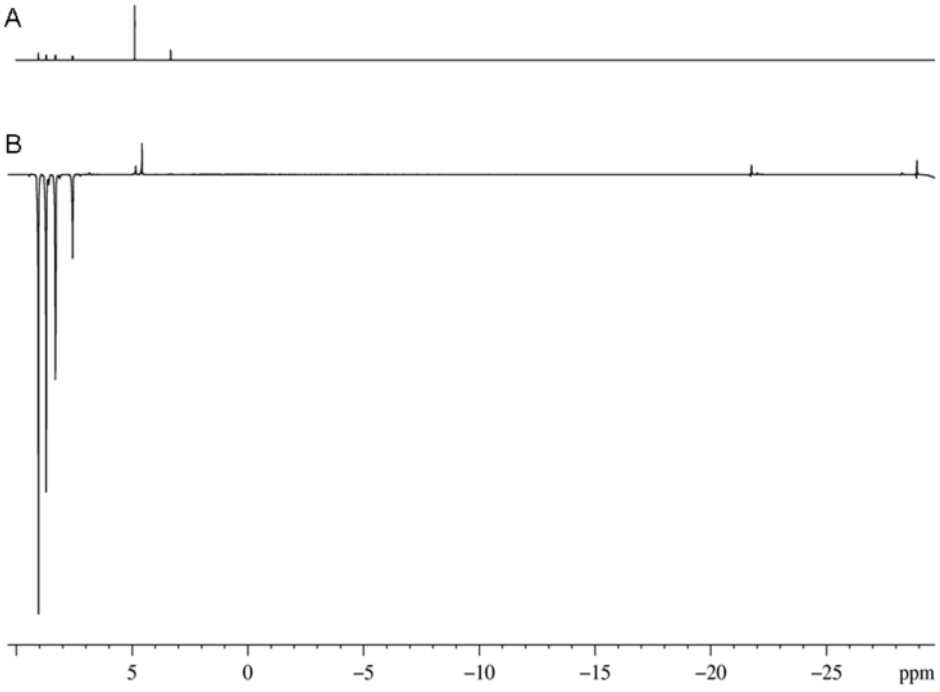

Figure S45. ^{1}H NMR spectra of a sample containing 0.1 M nicotinamide and 5 mol% 1 in MeOD-d_4 after; (A) thermal equilibrium at high field; and (B) polarization transfer from p-H_2 at 6.5 x10^{-3} T and 60°C

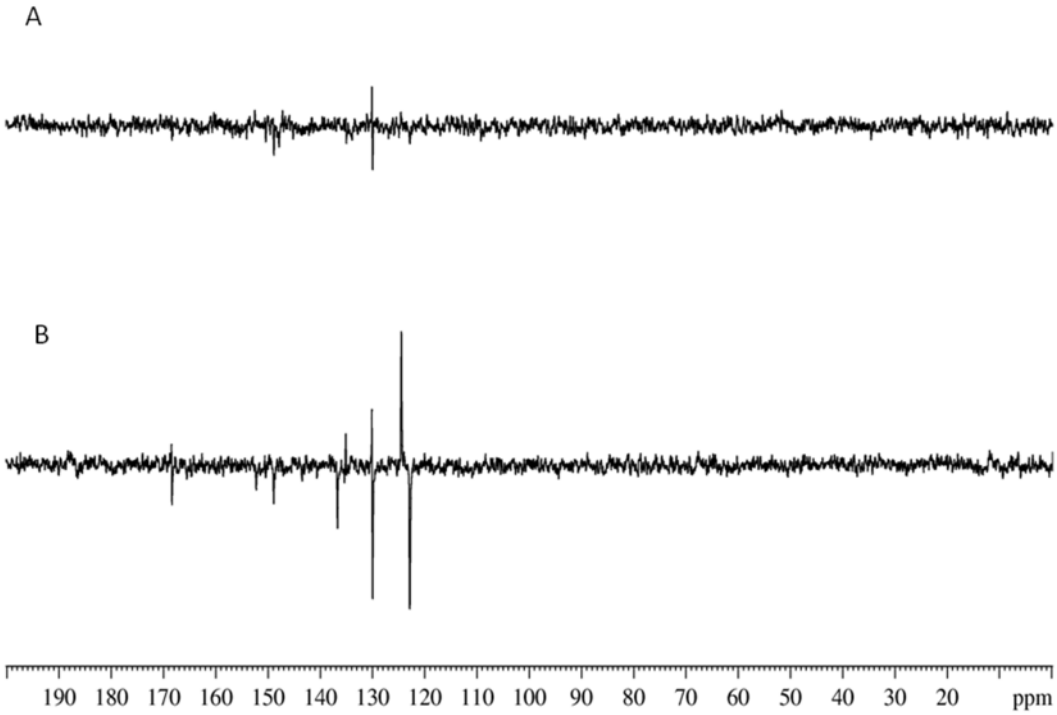

Figure S46. ^{13}C NMR spectra of a sample containing 0.1 M pyridine and 5 mol% 1 in MeOD-d_4 after polarization transfer from p-H_2 at 60°C and 2 x10^{-4} T (A) and 6.5 x10^{-3} T (B)

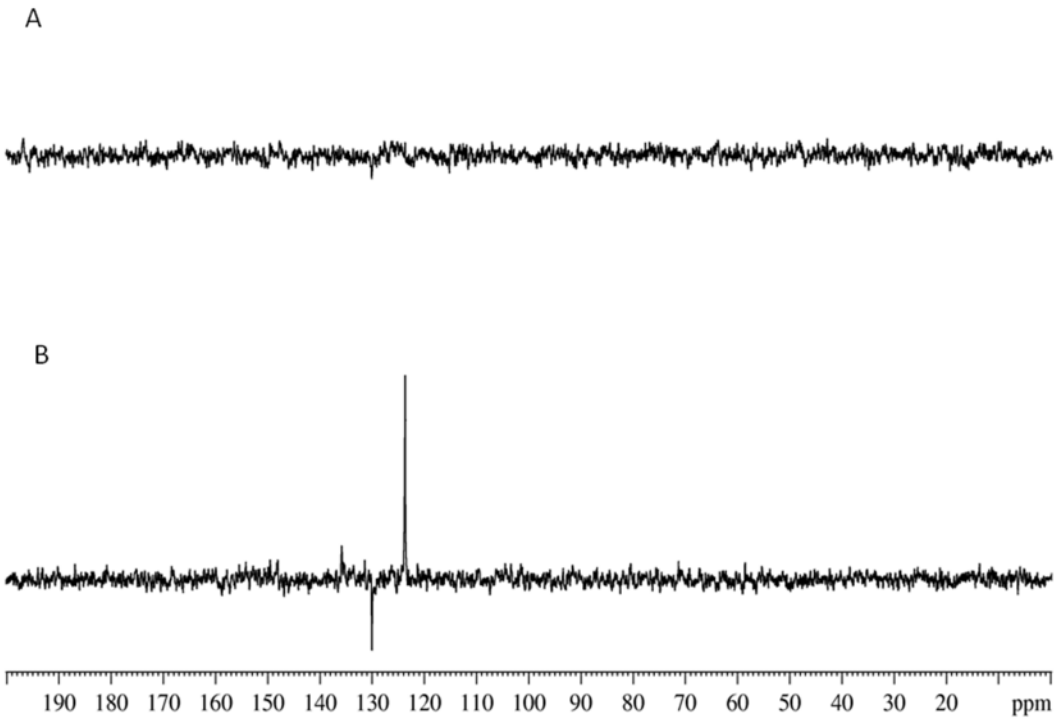

Figure S47. $^{13}C\{^1H\}$ NMR spectra of a sample containing 0.1 M nicotinamide and 5 mol% 1 in MeOD-d_4 after polarization transfer from p-H_2 at 60°C and 2 x10^{-4} T (A) and 6.5 x10^{-3} T (B)

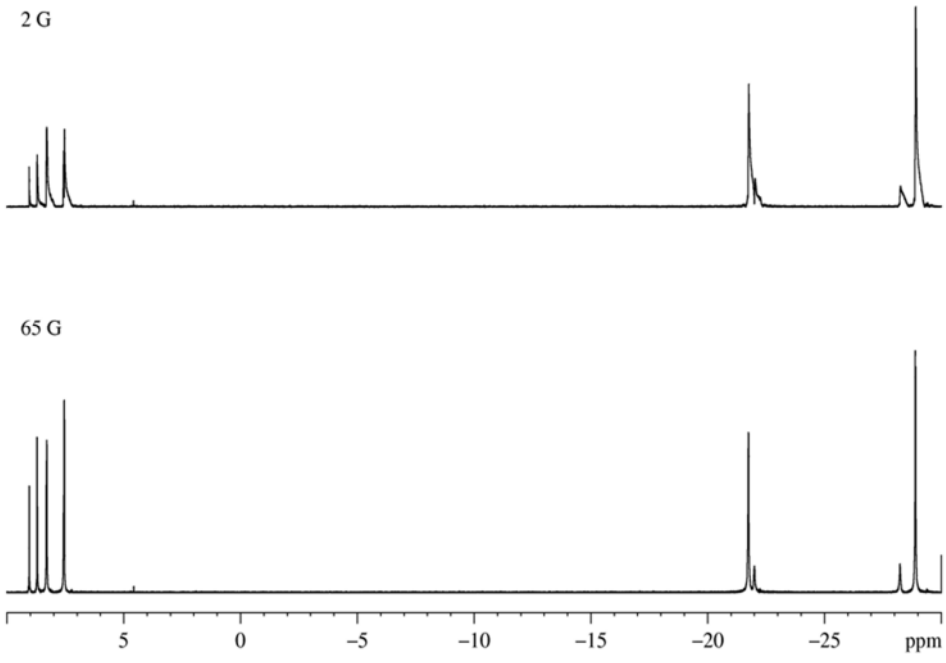

Figure S48. OPSY-dq ^1H NMR spectra of a sample containing 0.1 M nicotinamide and 5 mol% 1 in MeOD-d_4 after polarization transfer from p-H_2 at 60°C and 2 x10^{-4} T (A) and 6.5 x10^{-3} T (B)

Polarization transfer to nicotinamide using 1 as a catalyst using method B

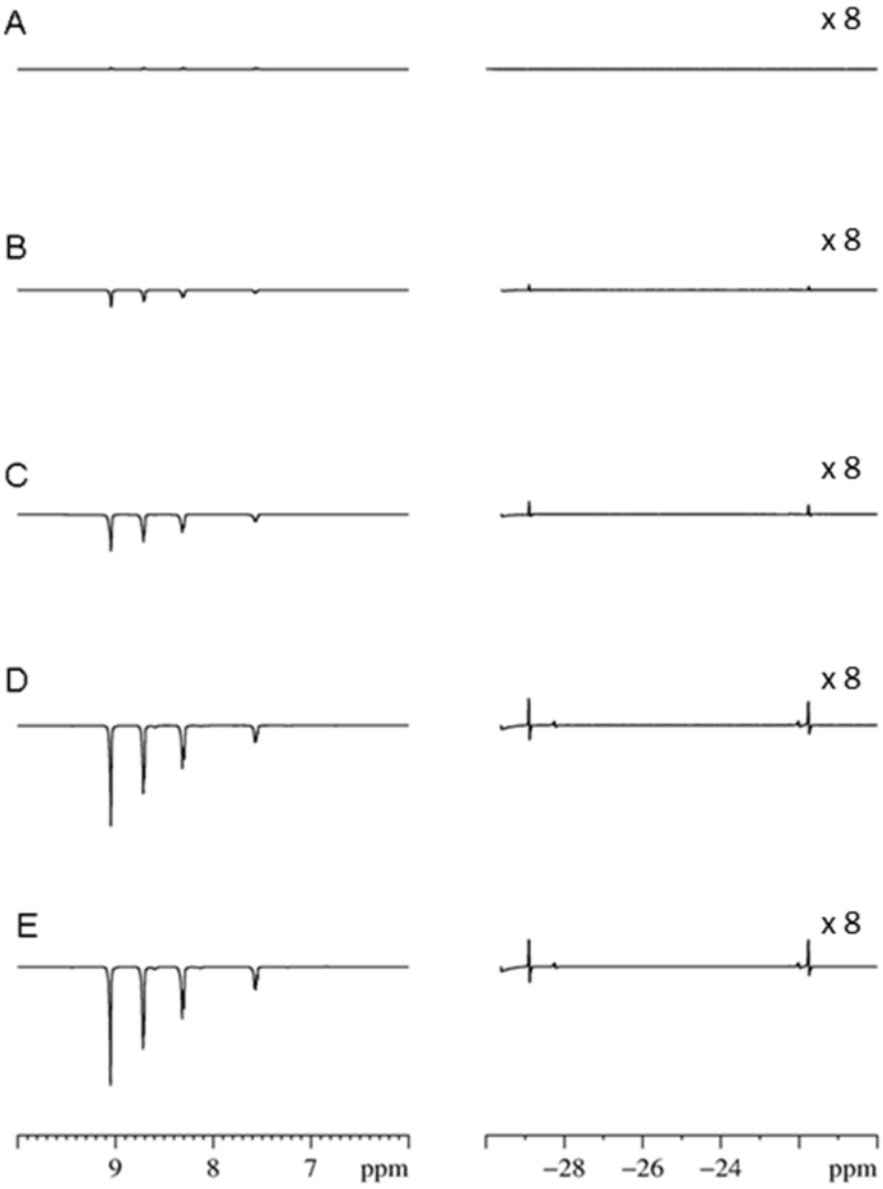

Figure S49. ^{1}H NMR spectra of a sample containing 0.1 M nicotinamide and 5 mol% 1 in MeOD-d_4 after polarization transfer from p-H_2 at 60°C and 6.5 x10^{-3} T. Between each run (A-E), the sample was cooled to RT before the process was repeated again

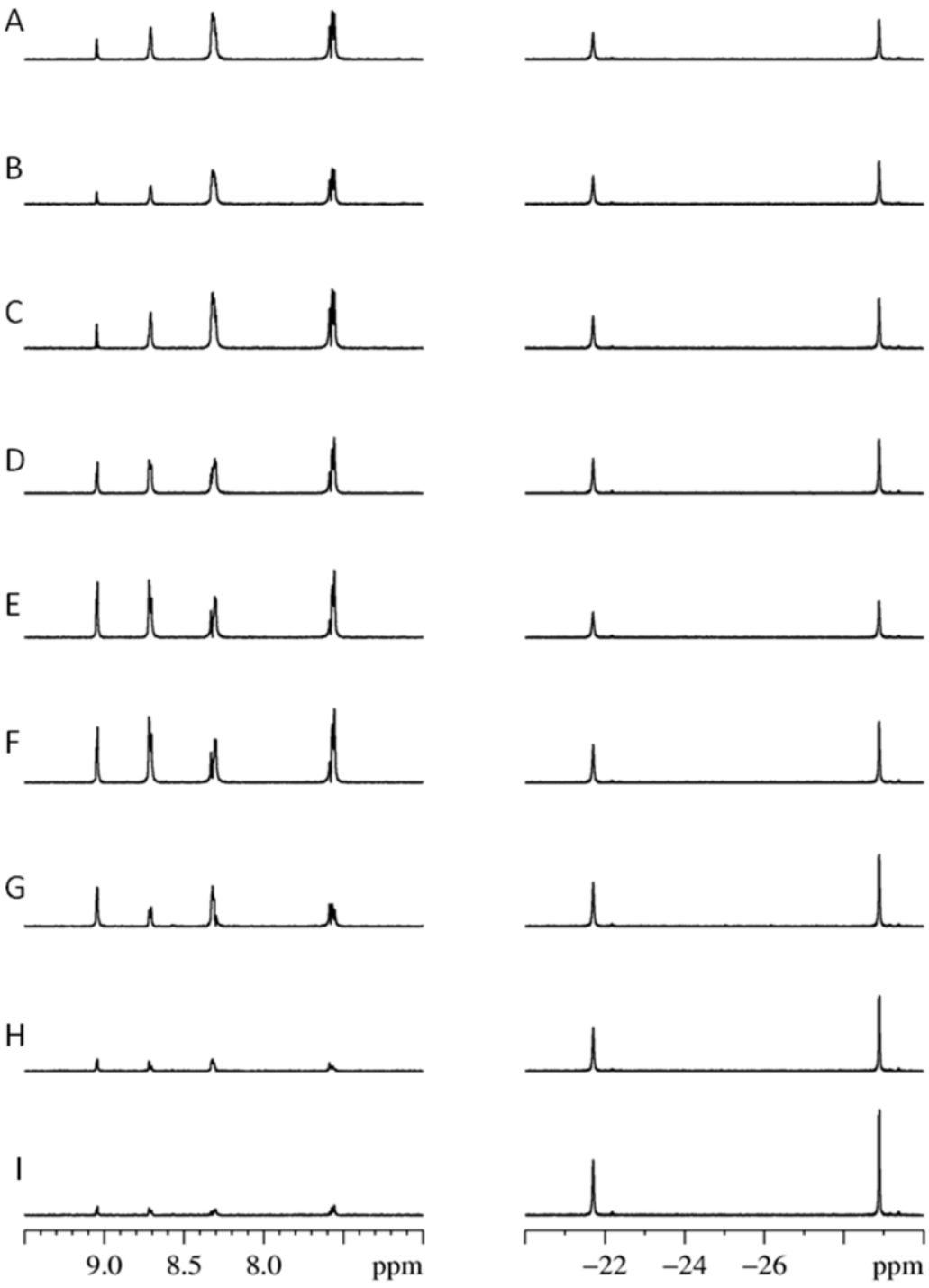

Figure S50. OPSY-dq ^{1}H NMR spectra of a sample containing 0.1 M nicotinamide and 5 mol% 1 in MeOD-d_4 after polarization transfer from p-H_2 at RT and 2.5 x10^{-3} T (A); 0 x10^{-4} T (B), −2.5 x10^{-3} T (C), −5 x10^{-3} T (D); −6.5 x10^{-3} T (E); −7.5 x10^{-3} T (F); −1 x10^{-2} T (G); −1.25 x10^{-2} T (H); −1.5 x10^{-2} T (I)

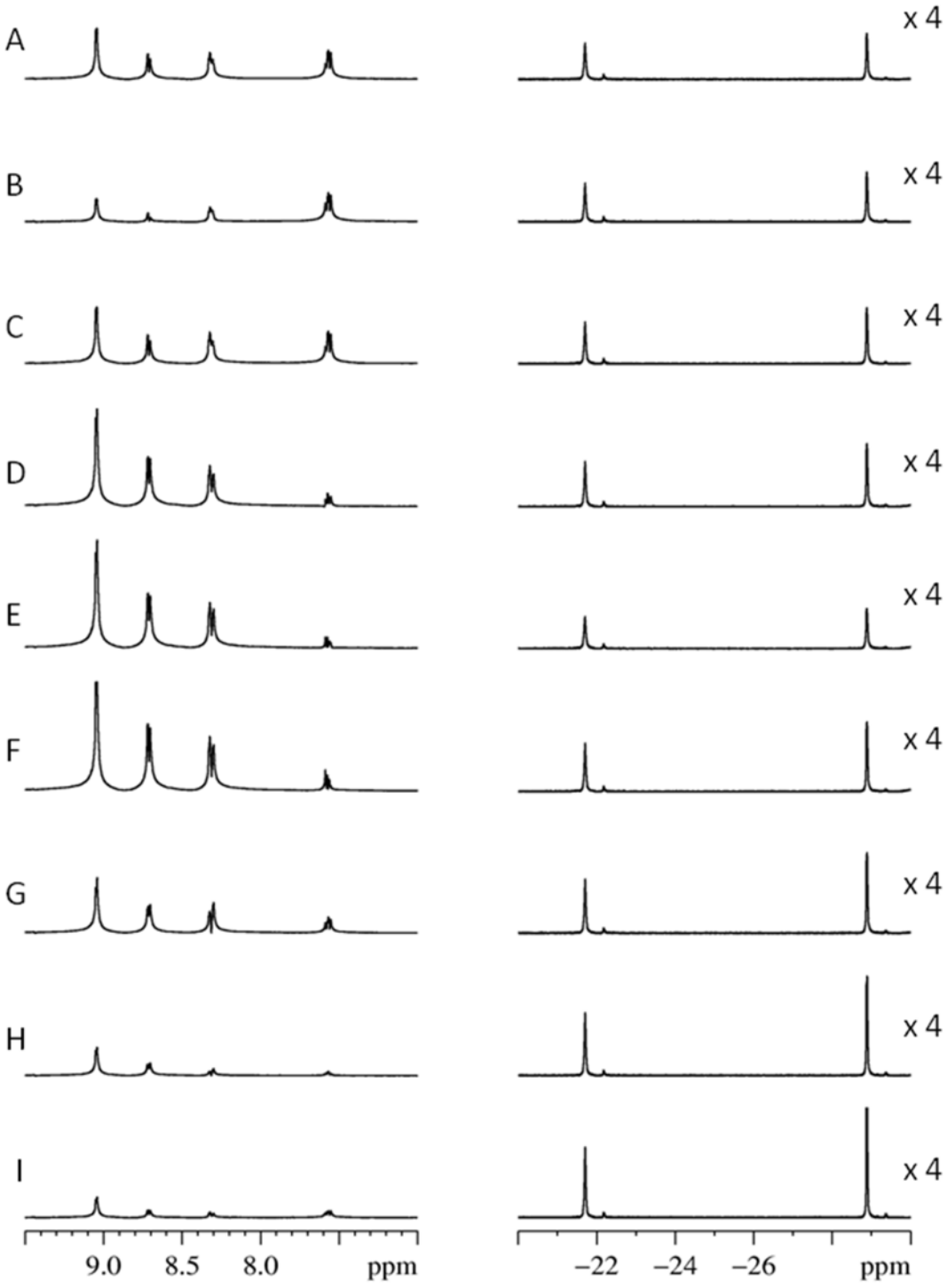

Figure S51. OPSY-zq ^{1}H NMR spectra of a sample containing 0.1 M nicotinamide and 5 mol% 1 in MeOD-d_4 after polarization transfer from p-H_2 at RT and 2.5 x10^{-3} T (A); 0 x10^{-4} T (B), −2.5 x10^{-3} T (C), −5 x10^{-3} T (D); −6.5 x10^{-3} T (E); −7.5 x10^{-3} T (F); −1 x10^{-2} T (G); −1.25 x10^{-2} T (H); −1.5 x10^{-2} T (I)

Influence of temperature on polarization transfer to nicotinamide using 1 as a catalyst using method A

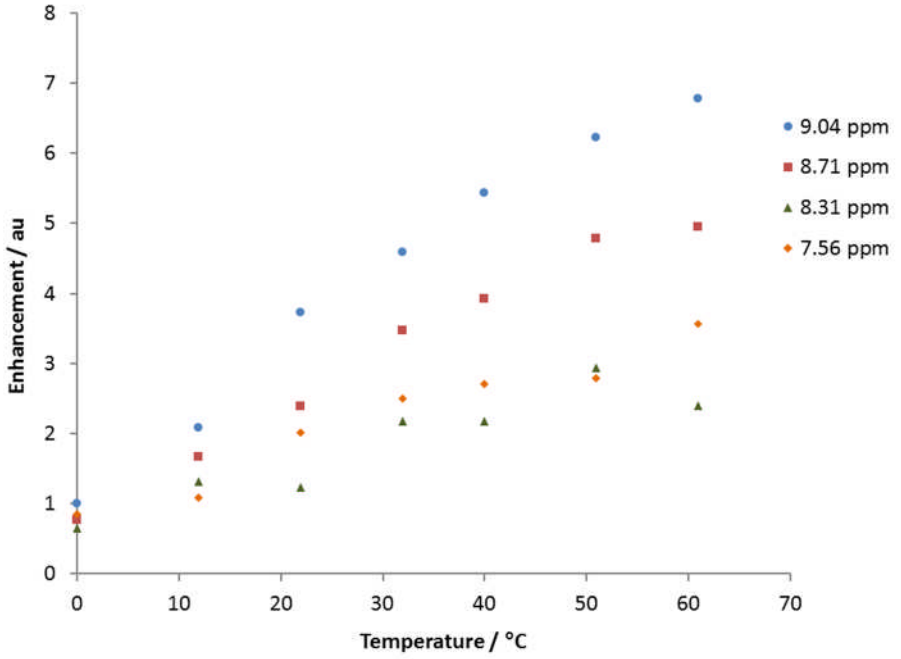

Figure S52. Enhancement observed for each type of ^{1}H resonance (H_A●, H_B▲, H_C♦, H_D■) of nicotinamide after polarization transfer from p-H_2 using 1 at 2 x10^{-4} T

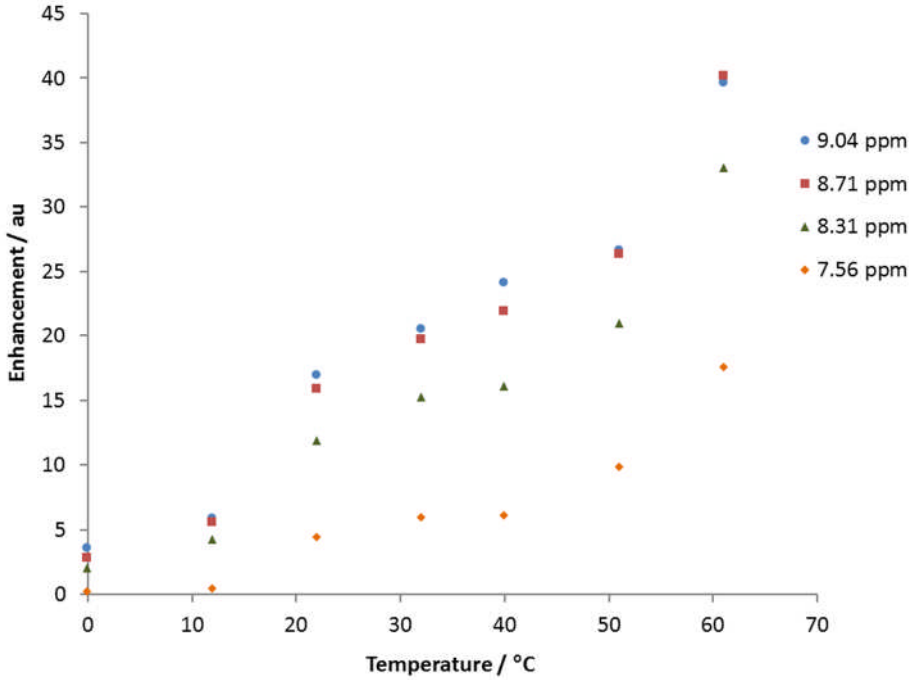

Figure S53. Enhancement observed for each type of ^{1}H resonance (H_A●, H_B▲, H_C♦, H_D■) of nicotinamide after polarization transfer from p-H_2 using 1 at 6.5 x10^{-3} T

Influence of temperature on polarization transfer to nicotinamide using 4 as a catalyst using method A

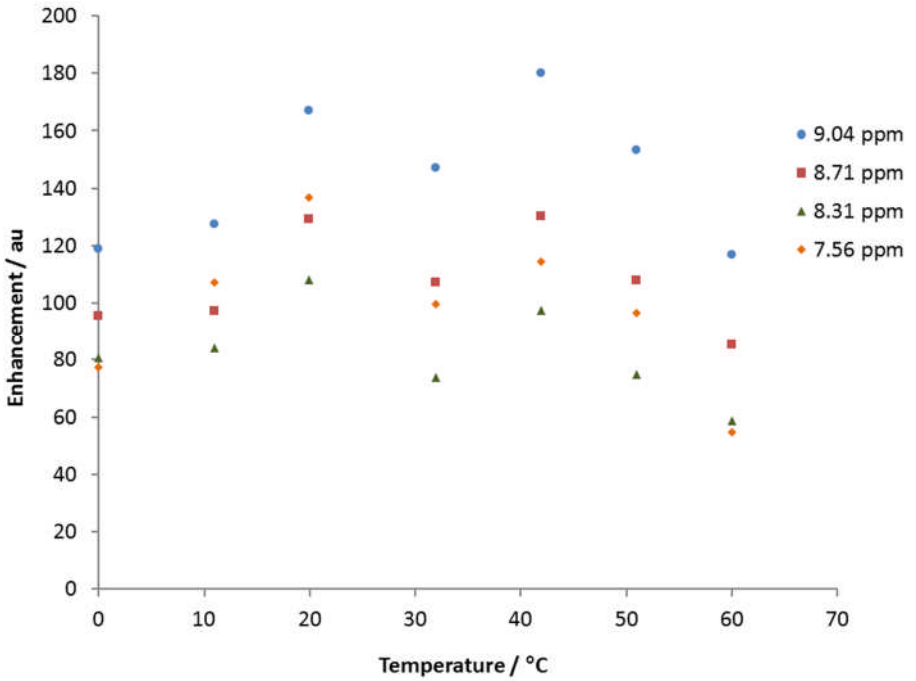

Figure S54. Enhancement observed for each type of ^{1}H resonance (H_A●, H_B▲, H_C♦, H_D■) of nicotinamide after polarization transfer from p-H_2 using 4 at 2 x10^{-4} T

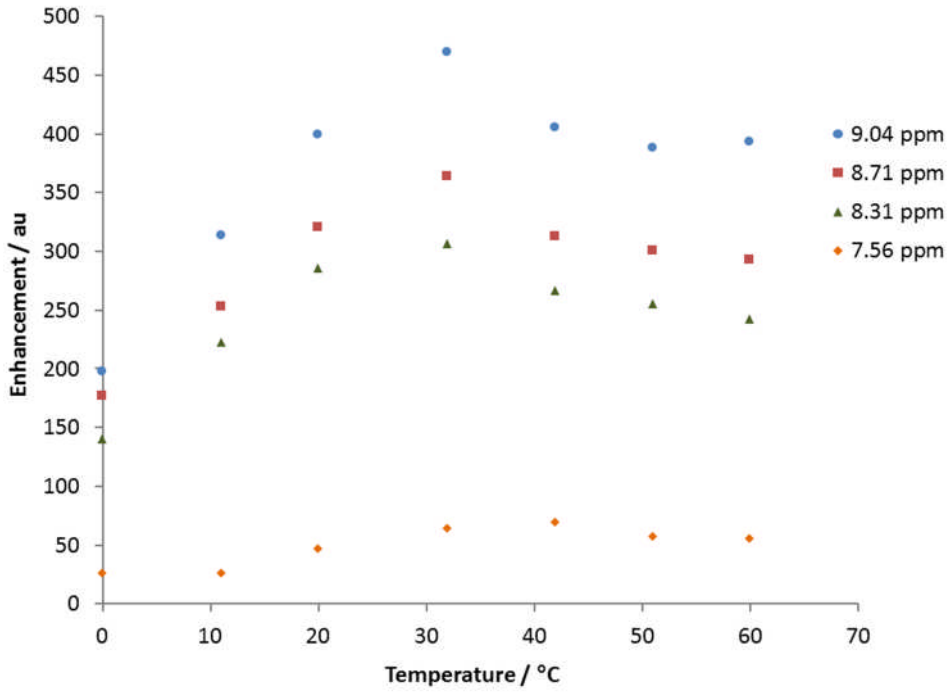

Figure S55. Enhancement observed for each type of ^{1}H resonance (H_A●, H_B▲, H_C♦, H_D■) of nicotinamide after polarization transfer from p-H_2 using 4 at 6.5 x10^{-3} T

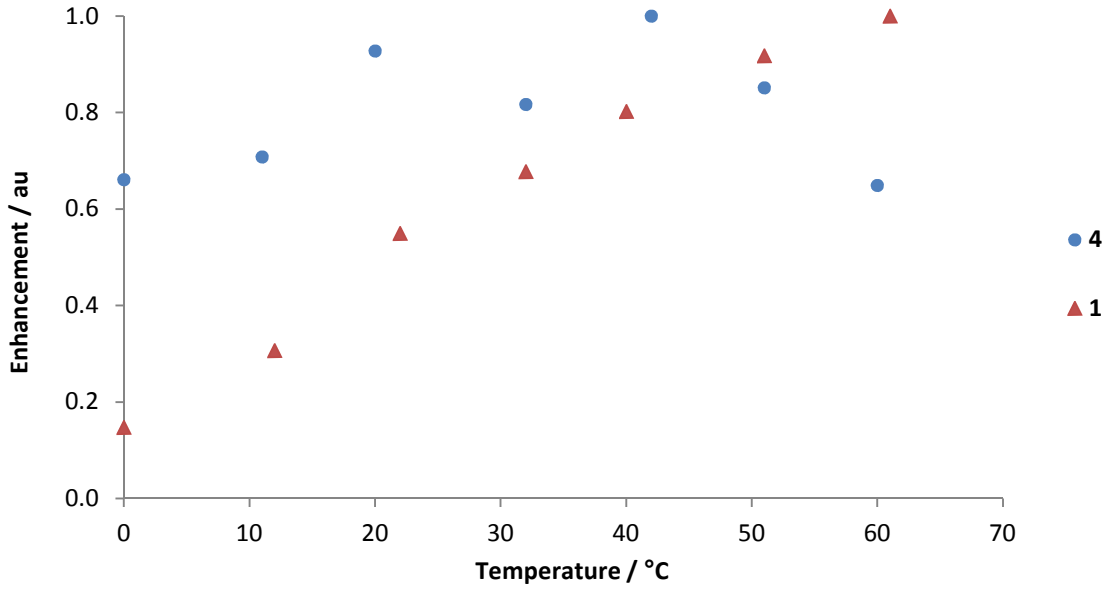

Figure S56. Normalised enhancement of the H_A ^{1}H NMR resonance of nicotinamide after polarization transfer using p-H_2 at 2 x 10^{-4} T; one containing nicotinamide (0.1M) and 4 (2 mg) in deuterated methanol (0.6 ml) and one containing nicotinamide (0.1M) and 1 (2 mg) in deuterated methanol (0.6 ml)

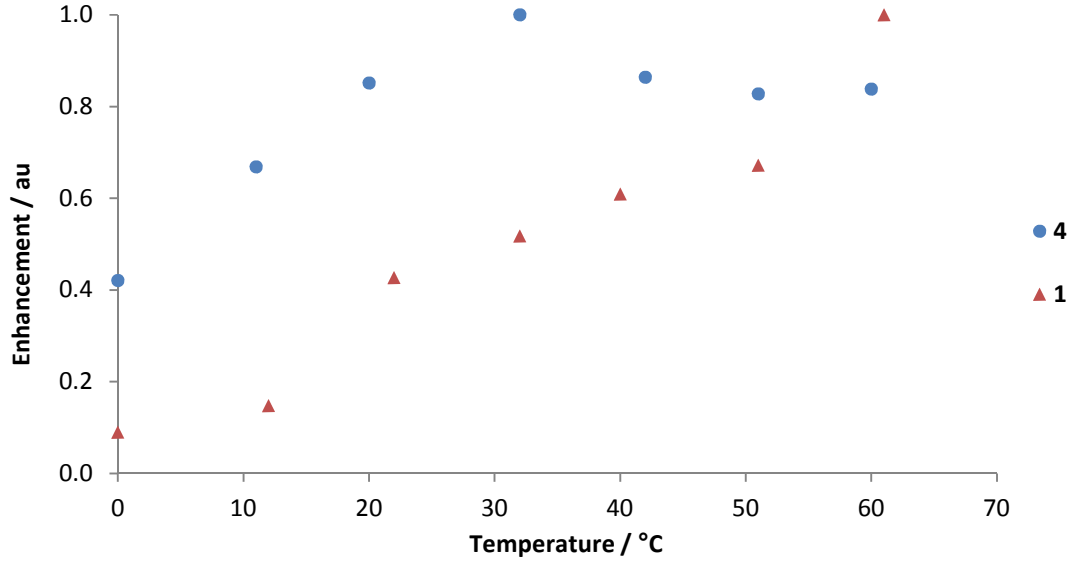

Figure S57. Normalized enhancement of the H_A ^{1}H NMR resonance of nicotinamide after polarization transfer using p-H_2 at 6.5 x 10^{-3} T; one containing nicotinamide (0.1M) and 4 (2 mg) in deuterated methanol (0.6 ml) and one containing nicotinamide (0.1M) and 1 (2 mg) in deuterated methanol (0.6 ml)

Examination of the effect of solvent on the reaction of 3 with *p*-H_2

The same active catalyst **3** formed in all solvents that were studied. SABRE was demonstrated in each solvent and the two inequivalent hydrides were present as shown in Figure S58. The proton NMR enhancement values for the protons of pyridine are shown in Table S27.

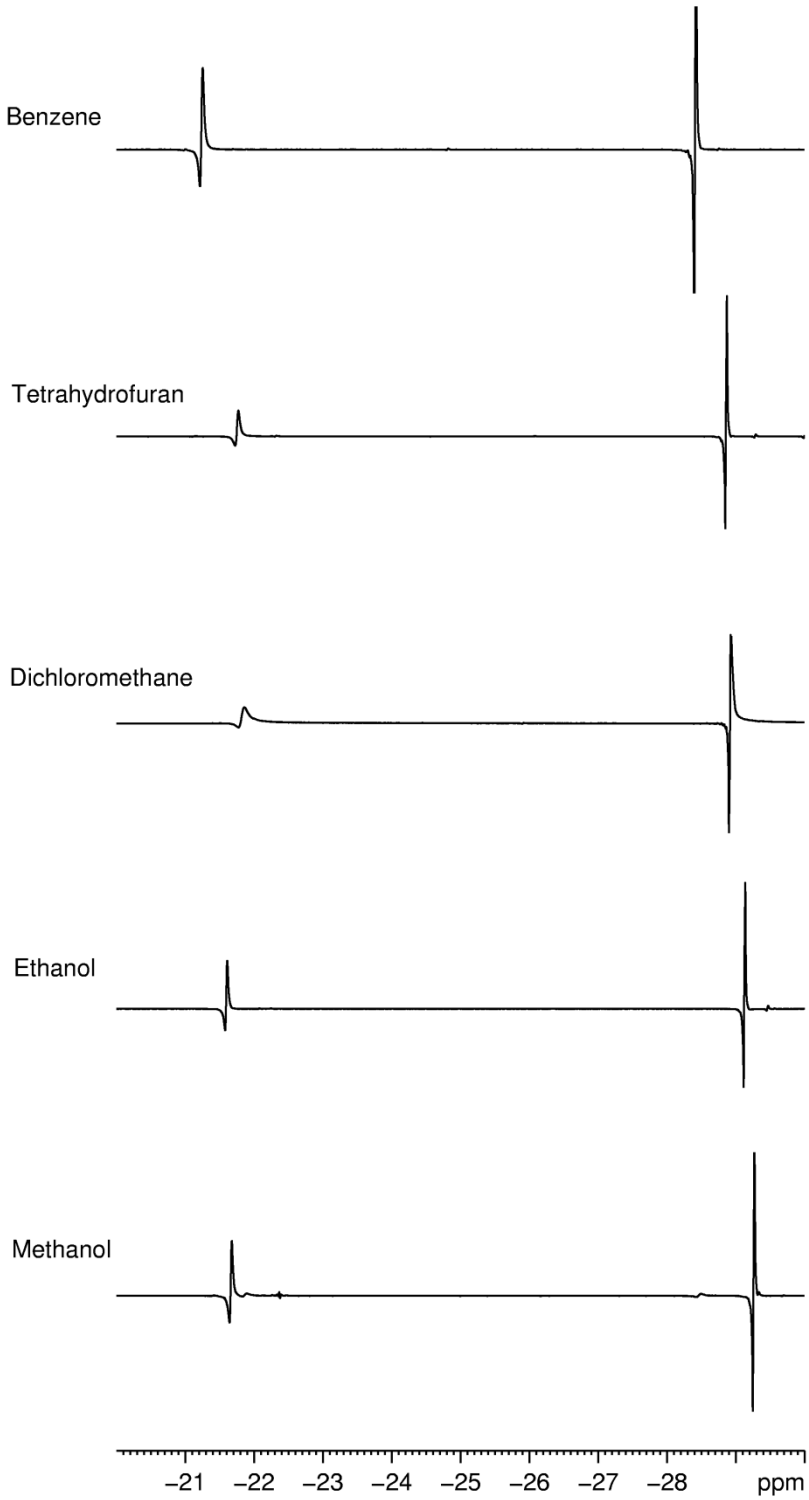

Figure S58. The hydride region of each spectra when polarizing pyridine in different solvents

Table S27. Pyridine ^{1}H NMR signal enhancements produced for a series of 0.05 M pyridine and 15 mol% 1 solutions at 298 K with 3 bar of p-H_2 after an activation period of 48 hours and 24 days

	Pyridine ^{1}H NMR SABRE enhancement (fold)					
Deuterated solvent	**48 hours**			**24 days**		
	ortho	***meta***	***para***	***ortho***	***meta***	***para***
Benzene	115.8 ± 6.1	89.9 ± 5.2	54.1 ± 3.0	501.5 ± 76.7	401.5 ± 87.1	222.0 ± 41.8
THF	93.6 ± 5.7	57.5 ± 4.9	46.9 ± 3.2	579.2 ± 24.1	402.1 ± 49.5	262.1 ± 11.8
CD_2Cl_2	132.5 ± 13.3	94.4 ± 15.9	60.6 ± 7.1	306.7 ± 58.1	222.1 ± 58.9	138.5 ± 26.7
Ethanol	72.5 ± 13.9	26.7 ± 8.2	30.5 ± 6.1	281.4 ± 28.7	135.0 ± 23.5	141.3 ± 7.5
Methanol	176.4 ± 9.1	122.6 ± 8.4	78.2 ± 4.0	27.4 ± 3.5	21.0 ± 3.5	16.7 ± 2.3

After long activation times, the complex also seemed to be stable in both CD_2Cl_2 and benzene. However, after 24 days the signal enhancements in methanol had severely dropped off. This relates to the ^{2}H-labelling of the pyridine due to H-D exchange with the solvent and incorporation into the *ortho* proton site of the pyridine; 50 % deuteration of the *ortho* proton signal for pyridine was observed after 24 days. It could also be due to instability of the samples in alcohol solvents after longer time periods as the sample degrades. The enhancements for the non-polar solvents are now much larger than for the polar solvents. This relates to the slower activation of the catalyst in non-polar solvents and the fact that deuteration does not occur in benzene or CD_2Cl_2. Slower activation is thought to occur due to the fact that non-polar solvents such as benzene cannot bind and be involved in the coordination sphere of the catalyst to aid activation.

7. References

(1) Harris, D. C., *J. Chem. Educ.* **1998,** *75*, 119-121.
(2) Arduengo, A. J., *III. U.S. Patent 5077414* **1991**.
(3) Occhipinti, G.; Jensen, V. R.; Törnroos, K. W.; Frøystein, N. Å.; Bjørsvik, H.-R., *Tetrahedron* **2009,** *65*, 7186-7194.
(4) Cowley, M. J.; Adams, R. W.; Atkinson, K. D.; Cockett, M. C. R.; Duckett, S. B.; Green, G. G. R.; Lohman, J. A. B.; Kerssebaum, R.; Kilgour, D.; Mewis, R. E., *J. Am. Chem. Soc.* **2011,** *133*, 6134-6137.